THE ASTROPHYSICAL JOURNAL, 445:246–268, 1995 May 20

ANATOMY OF THE GEMINI OB1 MOLECULAR CLOUD COMPLEX

JOHN M. CARPENTER,[1] RONALD L. SNELL, AND F. PETER SCHLOERB
Five College Radio Astronomy Observatory, Department of Physics and Astronomy,
University of Massachusetts at Amherst, Amherst, MA 01003;
carp@swas.phast.umass.edu
Received 1994 August 29; accepted 1994 November 23

ABSTRACT

We have investigated the large-scale morphology and properties of the molecular gas in the Gem OB1 cloud complex by mapping over 32 deg^2 (177 pc × 221 pc) of the complex in ^{12}CO(J = 1–0) and ^{13}CO(J = 1–0) at 50″ sampling with QUARRY on the FCRAO 14 m telescope. The most striking characteristic of the molecular line images are the series of arc- and ring-shaped structures found on spatial scales from a few parsecs in diameter up to at least 35 pc. The morphology and in some instances the kinematics suggest that these features represent swept-up molecular material, most likely from expanding H II regions and wind blown bubbles. The kinetic temperatures and column densities of the molecular gas were derived from the ^{12}CO and ^{13}CO data using the LTE analysis. Most of the molecular gas was found to have kinetic temperatures of $\lesssim$10 K, and 50% of the mass of gas is contained in lines of sight with H_2 column densities $\lesssim 2 \times 10^{21}$ cm^{-2}. It was found that only 10% of the molecular mass is contained in lines of sight with column densities in excess of 10^{22} cm^{-2}, and that these regions are found almost exclusively near the massive star forming regions within the arcs and rings of molecular gas. The average H_2 densities in areas with ^{13}CO emission are between 65–120 cm^{-3}, consistent with previous studies of cloud complexes, and is independent of whether the regions contains massive star formation or not. For the Gem OB1 complex as a whole, the average H_2 density is 1.2 cm^{-3}, which is only a few times the average atomic hydrogen density in the interstellar medium.

We suggest an overall picture for the Gem OB1 complex in which most of the molecular gas is contained in relatively cold, low column density molecular material. The high column density regions in the Gem OB1 complex form through the external compression of the molecular gas by the winds and H II regions from newly formed massive stars. Thus once massive star formation is initiated, the structure and further evolution of the cloud complex is largely a result of the interactions of expanding H II regions and stellar winds with the ambient molecular material.

Subject headings: H II regions — ISM: clouds — ISM: individual (Gemini OB1) — ISM: molecules — ISM: structure

1. INTRODUCTION

Despite the fact that molecular gas in the Galaxy has been extensively studied for over 20 years, recent evidence indicates that the observational description of the molecular interstellar medium remains vastly incomplete (Scalo 1990). From small clumps in Taurus (Falgarone, Phillips, & Walker 1991) to the long narrow filaments found throughout the Orion cloud complex (Bally et al. 1987), molecular gas in the interstellar medium contains highly intricate structures that imply the presence of dynamic forces operating over several orders of magnitude in spatial scales. While the largest single-dish telescopes continue to probe the structure of the molecular gas on size scales of a few thousand AU in nearby cloud complexes, the primary limitation in further characterizing the large-scale structure of the molecular gas has been the inordinate amount of time required to map large regions of the sky at high angular resolution. Time constraints limit most detailed studies to small regions within molecular cloud complexes, and more often than not, to areas with known star forming sites at the expense of more extended gaseous components. Thus it remains unclear to what extent the observed filamentary and clumpy structures represent intrinsic properties of the molecular gas or byproducts of star formation events. In principle, extensive molecular line surveys remove many of these biases, but in practice most surveys to date have lacked the angular resolution and sampling to resolve many of the large-scale features, and thus may not provide an adequate representation of the large-scale structure of molecular gas.

We have begun to address many of these issues by conducting an extensive investigation of the molecular gas and star-formation activity near the Gem OB1 association. The Gem OB1 association lies toward the anticenter region of the Galaxy at (l = 189°, b = 1°), with the associated molecular gas spanning a 6° × 6° region on the sky (Huang & Thaddeus 1986). The distinguishing characteristic of this investigation compared to previous large-scale studies of molecular cloud complexes (Bally et al. 1987; Heyer et al. 1992; Xie & Goldsmith 1994; Lee, Snell, & Dickman 1994) is the spatial scale covered by these observations. The images of the Gem OB1 complex presented here cover an area of 177 × 221 pc at 0.48 pc sampling, which probes the structure of the molecular interstellar medium on spatial scales several times larger than the extensive studies of Orion (Bally et al. 1987; Heyer et al. 1992) and Mon R2 (Xie et al. 1993). Thus this study can place the smaller scale structures in a global context, which may lead to information on their formation and evolution. Furthermore, while the Gem OB1 complex contains several distinct sites of massive star formation in addition to the OB association, there are large expanses of the complex that are not currently forming massive stars. Thus this study can potentially contrast

[1] Postal address: Institute for Astronomy, University of Hawaii, 2680 Woodlawn Drive, Honolulu, HI 96822; carp@galileo.ifa.hawaii.edu.

the morphology and properties of molecular gas in a range of stellar environments.

The salient result from this investigation is that much of the cloud structure and the embedded star formation activity in the Gem OB1 cloud complex can be attributed to the interaction of massive stars with the ambient molecular cloud through stellar winds and H II regions. This paper describes the large-scale morphology and properties of the Gem OB1 cloud complex that led to this conclusion, while a companion paper (Carpenter, Snell, & Schloerb 1995) examines the distribution of dense cores and embedded star-forming regions based on CS ($J = 2$–1), *IRAS*, and near-infrared observations. The details of the molecular line observations and data reduction procedures relevant to this paper are described in § 2. An overview of the Gem OB1 region is given in § 3, followed by a detailed discussion on the global morphology and kinematics of the Gem OB1 cloud complex in § 4 as revealed by the ^{12}CO and ^{13}CO data. In § 5, the techniques adopted to extract quantitative information on the molecular gas properties are reviewed, and are used in §§ 6 and 7 to determine the energetics, kinetic temperatures, and column densities of the molecular gas in the Gem OB1 complex. A summary of our conclusions is presented in § 8.

2. OBSERVATIONS AND DATA REDUCTION

The Gem OB1 complex was mapped in ^{12}CO($J = 1$–0) (115.271203 GHz) and ^{13}CO($J = 1$–0) (110.201370 GHz) between 1991 March and 1992 May with the FCRAO 14 m telescope using QUARRY (Erickson et al. 1992). The beam size of the 14 meter antenna at these transitions is 45″ and 47″ for ^{12}CO and ^{13}CO respectively. QUARRY contains 15 elements arranged in a 3 × 5 grid. The angular spacing of the beams on the sky is 100″ along the short axis of the array and 50″ along the long axis. The 100″ gap was filled in by shifting the array 50″ in declination, so that all of the maps presented here are nearly full-beam sampled. The data were taken in position switching mode and calibrated with the standard chopper wheel method of observing an ambient temperature load and sky emission. To increase the mapping efficiency, calibration and reference position measurements were obtained every 1.5 to 2 minutes after several on-source integrations. The back ends for each pixel of the array consisted of a two, 32 channel filter bank spectrometers, one with a channel resolution of 250 kHz (0.65 km s^{-1} for ^{12}CO) and the other with 1 MHz. Unless specifically stated, the maps presented here were made using the 250 kHz data.

The observed antenna temperatures corrected for the atmosphere and telescope losses are presented as T_R^* following the nomenclature recommended by Kutner & Ulich (1981). The spillover and scatter efficiency ($\eta_{\rm fss}$) of the telescope and radome has been determined from previous FCRAO measurements to be ~0.7 at these frequencies. A further correction, the source coupling efficiency (η_c), is needed to account for the coupling of the beam to the source. For a uniform source that fills only the main beam of the 14 m telescope, η_c is ~0.7 (i.e., 30% of the power is scattered on angular sizes much greater than the FWHP beam size), while for sources with uniform intensity over a diameter of 30′, η_c is 1.0. In practice, the observed structures in the ^{12}CO and ^{13}CO maps span a range of sizes and shapes, and so applying a single coupling efficiency for the entire map is incorrect. Rather than attempt to apply the coupling coefficient on a pixel by pixel basis, the data are presented in T_R^* temperature units. The ^{12}CO map contains 175,200 spectra covering a 5.°07 × 6.°67 region with a typical rms of $\Delta T_R^* \sim 0.6$ K, while the ^{13}CO map contains 166,440 spectra over a 5.°07 × 6.°33 region with a rms of ~0.3 K. The ^{12}CO map is slightly extended in declination both north and south of the ^{13}CO map to completely map a feature in the southern portion of the cloud complex and to cover the IC 443 region.

3. OVERVIEW OF THE GEMINI OB1 CLOUD COMPLEX

The identification of the Gem OB1 association stems from a concentration of bright O and B stars extending from $l \sim 187°$ to 191° and from $b \sim -2°$ to 4°. Hardie, Seyfert, & Gulledge (1960) identified 58 possible association members, and Barbaro, Dallaporta, & Fabris (1969) estimated an age of 10 Myr for the association based on the main-sequence turnoff in the HR diagram. Considerable age spread exists among the association members. For instance, Grasdalen & Carrasco (1975) estimate an age of only 2 Myr for the cluster of stars surrounding the O6.5 star HD 42088 in Sh 252. The average distance to the association based upon spectroscopic and photometric observations is 1.5 kpc (see the discussion in the Appendix).

Figure 1 presents a schematic of the various optical objects located near the Gem OB1 association together with a coarse ^{12}CO contour map. The circles represent the approximate sizes

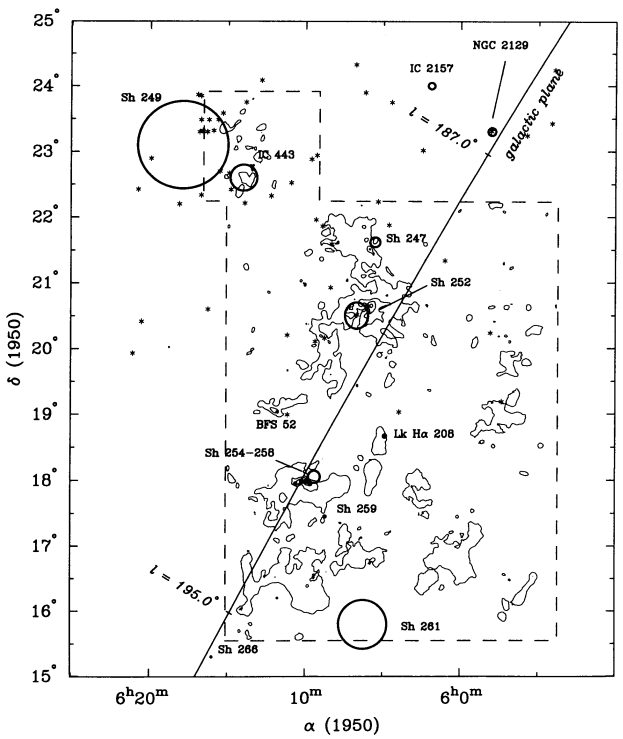

FIG. 1.—Schematic of the various optical features in relation to the molecular gas. The dashed line delineates the region mapped in ^{12}CO, and the contour represents the observed ^{12}CO emission. The solid circles mark the location and sizes of optical H II regions, supernova remnants, and open clusters, and the asterisks (*) the location of possible members of the Gem OB1 association (Crawford et al. 1955; Hardie et al. 1960; Humphreys 1978). As discussed in the text, some of these features are likely background and foreground objects, most notably LkHα 208 and Sh 259. Note that the right ascension range shown is strictly correct only for a declination of 18° (the origin of the map), as the coordinate grid shown in this figure and all other such figures in this paper neglect the curvature of the sky in the equatorial coordinate system.

and locations of cataloged nebulae (Sharpless 1959; Blitz, Fich, & Stark 1982), supernova remnants, and open clusters, and the asterisks (*) signify positions of possible members of the Gem OB1 association (Crawford et al. 1955; Hardie et al. 1960; Humphreys 1978). The dashed line marks the extent of the region mapped in ^{12}CO. The optical nebula found within the body of the molecular gas include the supernova remnant IC 443, the bipolar reflection nebula LkHα 208, and the H II regions BFS 52, Sh 247, Sh 252, the Sh 254, Sh 255, Sh 256, Sh 257, and Sh 258 group (hereafter referred to as Sh 254–258), Sh 259, and Sh 261. Of these objects, LkHα 208 is likely associated with foreground molecular material as based on extinction evident on the Palomar prints, and Sh 259 is likely a background H II region (see the Appendix). The greatest concentration of OB stars is in the IC 443/Sh 249 region, which is offset from the bulk of the molecular gas.

The original identification of the Gem OB1 molecular cloud complex stems from the Columbia ^{12}CO survey of the Galactic plane (Dame et al. 1987; see also Blitz 1978; Huang & Thaddeus 1986; Leisawitz, Bash, & Thaddeus 1989; Stacy & Thaddeus 1991). The ^{12}CO maps of this region show an enhancement of molecular gas near the Gem OB1 association, and based on the paucity of molecular gas in general toward the outer Galaxy, it seems likely that most of the molecular gas would be at roughly the same distance. More substantial evidence comes from observations of Sh 247, Sh 252, and Sh 254–258. Each of these H II regions have spectroscopic and photometric distance estimates of $\sim$2.0 kpc (see the Appendix). Since these H II regions are associated with a large fraction of the molecular gas in the mapped region, these distance estimates form the primary justification for treating the Gem OB1 cloud complex as a single entity. While the estimated distance to the Gem OB1 association of 1.5 kpc (Humphreys 1978) differs from that of the molecular gas, it is not clear how significant this difference is given the potential for systematic errors in both distance estimates. Throughout this paper, we adopt the distance to the cloud complex that is most directly related to the molecular gas, 2.0 kpc.

Distance estimates toward the molecular gas along the western and southern edges of the Gem OB1 cloud complex are not as readily available since no optically visible H II regions are present in these two areas. Based on a possible morphological connection between the western edge of the Gem OB1 complex and the Gem OB1 association (see § 7) and a possible relationship between the southern edge of the Gem OB1 cloud complex and the H II region Sh 261 which has a spectroscopic distance estimate of 1.8 kpc, these two regions are also considered as part of the Gem OB1 complex. It is possible, however, that these regions may be as close as 1.0 kpc, as discussed in the Appendix.

4. MORPHOLOGY OF THE GEM OB1 CLOUD COMPLEX

Figures 2*a* and 2*b* present full resolution gray-scale images of the peak ^{12}CO and ^{13}CO antenna temperature, respectively, of the Gem OB1 cloud complex. Maps of the average antenna temperature in 2 km s^{-1} bins (i.e., three channels in the spectrometer) for both ^{12}CO and ^{13}CO are shown in Figure 3. The northern extension of the ^{12}CO map outlined in Figure 1 covers IC 443 and is discussed in § 4.4. The brightest molecular emission is found near the optical H II regions Sh 247, Sh 252, and Sh 254–258 with additional regions of extended, strong molecular emission along the western edge and southern quarter of the cloud complex. As expected, the ^{12}CO emission is much more spatially extended than the ^{13}CO emission, as it is more sensitive to low column density molecular gas.

Even the most cursory examination of the peak antenna temperature images and the maps at individual velocities reveals a highly intricate morphology to the Gem OB1 molecular cloud complex. Long, narrow, filamentary shaped structures, loops and arcs, bright rims, and diffuse patchy regions are all readily observable. The following discussion describes these various features, and presents morphological and in some instances kinematic evidence that strongly suggests that many of these features have formed as a result of interactions of stars with the ambient molecular gas through expanding H II regions and stellar winds.

4.1. *Sh 247*

The molecular gas near the optical H II region Sh 247 contains the most complex kinematic and spatial structure of all the large concentrations of molecular emission that were found. To better relate this structure to the extent of the optical H II region, Figure 4 displays the peak ^{13}CO antenna temperature image overlaid on the red Palomar Sky Survey print. The Sh 247 H II region has an angular diameter of $\sim$8′ and contains an exciting star of spectral type B0 V (Hunter & Massey 1990). At least three spatially distinct filaments are observed in this region. One filament at a velocity of $\sim$2 km s^{-1} wraps around the eastern edge of Sh 247 and is almost certainly physically associated with the H II region. The brightest molecular emission in the Sh 247 region occurs directly adjacent to the optical nebula in two compact peaks. The northeast corner of the optical nebula contains a straight edge, indicating where the H II region is bounded by the molecular gas or where the molecular gas wraps in front of the optical nebula. The second prominent filament also has a velocity of $\sim$2 km s^{-1} and lies $\sim$10′ further east with a similar size as the first filament, but instead curves away from Sh 247 and has no clear association with an optical object. A third filament is found at velocities between $\sim$10–12 km s^{-1} (see Fig. 3) and extends down to the Sh 252 region. The northern extent to this structure terminates near the southern edge of the second filament mentioned above (see also Kömpe et al. 1989).

4.2. *Sh 252*

The molecular gas around the Sh 252 H II region contains similar structural features as the gas around Sh 247. Figure 5 shows the peak ^{13}CO antenna temperature map overlaid on the red Palomar Sky Survey print for Sh 252. The main exciting star for the H II region, the O6.5 V star HD 42088, is located near the center of the nebula at (α, δ) = ($6^h06^m40^s.85$, 20°29′51″.4). An obvious cavity in the molecular gas exists where the optical nebula is situated. Portions of both the eastern and western edges of the nebula are sharply bounded by the molecular gas, which either indicates an ionization bounded H II region or that the cloud wraps in front of Sh 252 and obscures the nebular emission. Most of the ^{12}CO and ^{13}CO emission detected toward Sh 252 probably originates predominantly from the backside of the H II region since there is no evidence of extinction that correlates with the molecular emission (see also Grasdalen & Carrasco 1975). As in Sh 247, the general morphology strongly suggests a physical interaction between the H II region and the ambient molecular material, although as was the case for Sh 247, the velocity field of the molecular gas show no compelling evidence for overall expansion.

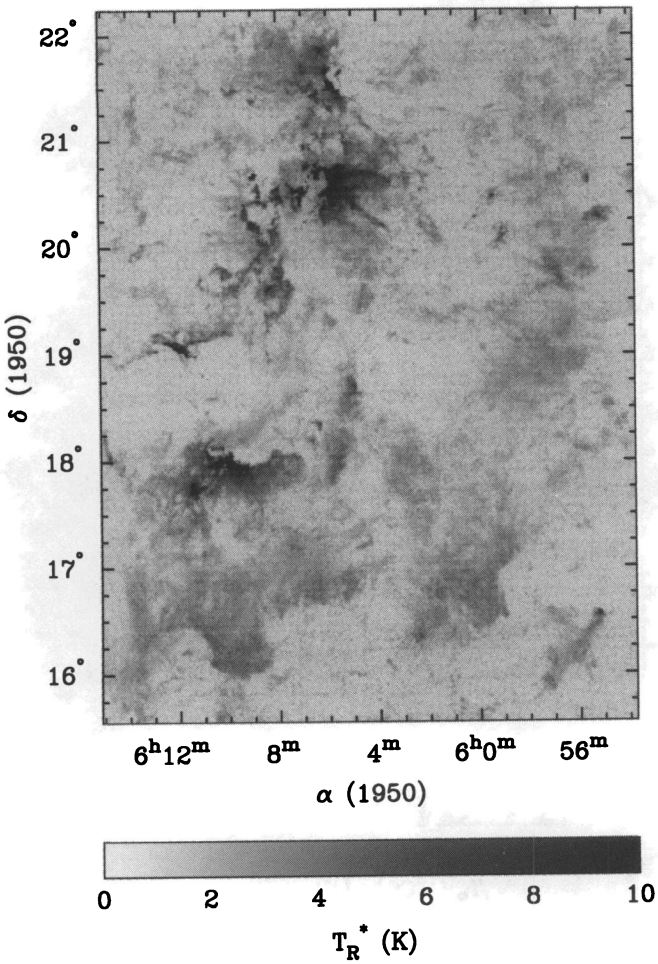

FIG. 2a

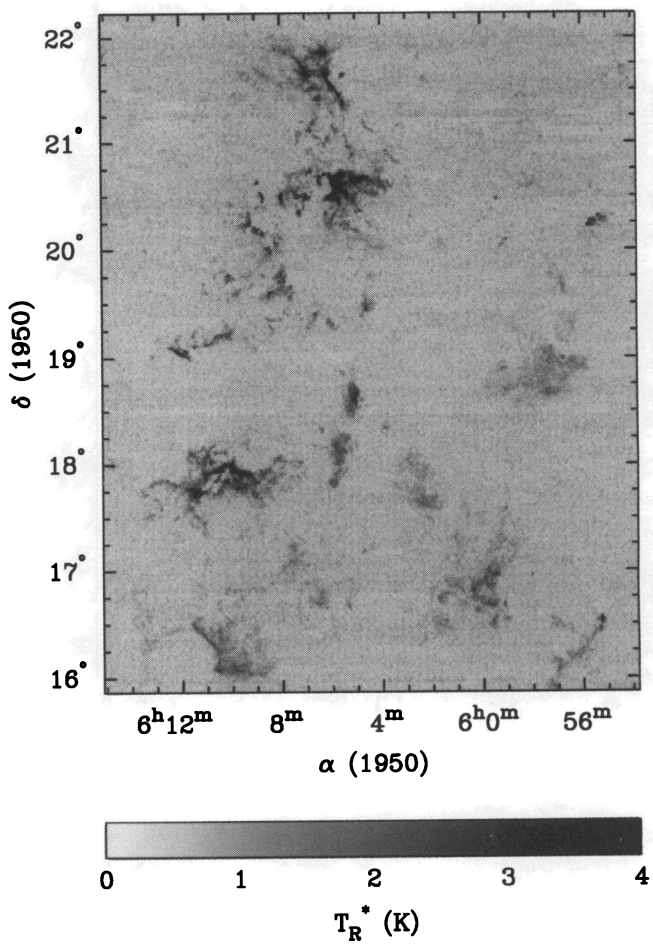

FIG. 2b

FIG. 2.—(*a*) Full resolution, gray-scale image of the observed peak $^{12}CO(J = 1–0)$ antenna temperature toward Gem OB1. (*b*) Full resolution, gray-scale image of the observed peak $^{13}CO(J = 1–0)$ antenna temperature toward Gem OB1.

Southeast of the Sh 252 H II region are three rings of ^{12}CO emission that are most readily apparent in the peak ^{12}CO antenna temperature image (Fig. 2*a*). Each of these rings has a diameter of ~15′ (9 pc). Stellar winds and expanding H II regions are obvious candidates for the origin of these rings, but no bright stars, stellar clusters, or *IRAS* point sources exist near the center of the rings. To examine the kinematics of these features, we compared the spectrum obtained by averaging the emission around the edge of the ring to that obtained by averaging all of the spectra at the ring center. While the emission toward the center of the rings are weak and most individual lines of sight have less than a 3 σ ^{12}CO detection, the averaged spectrum contains a reasonable signal to noise. Figure 6 compares these spectra in the northern most of the three large rings at $(\alpha, \delta) = (6^h9^m, 20°20')$. The solid histogram in Figure 6 is the ring-center averaged spectrum, and the dotted histogram represents the ring-edge averaged spectrum scaled by $\frac{1}{3}$. The ring-edge spectrum has a single emission peak, while the ring-center spectrum contains a nearly symmetric double peaked line profile with a peak to peak separation of ~4.5 km s^{-1} centered on the velocity of the ring-edge averaged spectrum. This is the kinematic signature of an expanding shell of molecular gas. The double peaked line profile toward the ring center represents the approaching (front) and receding (back) parts of the shell, while the motion of the gas on the perimeter of the shell is mostly tangential to the line of sight and thus not Doppler shifted.

4.3. *Sh 254–258*

As with Sh 247 and Sh 252, the molecular gas near Sh 254–258 group of optical nebula possesses structural features suggesting an interaction with the H II regions. Figure 7 shows an overlay of the ^{13}CO emission on the red Palomar Sky Survey prints of this region. Again, the molecular emission outlines the boundary of the largest optical H II region in this group, Sh 254. The strongest molecular emission occurs on the edge of Sh 254 and directly between Sh 255 and Sh 257 (see also Evans, Blair, & Beckwith 1977; Heyer et al. 1989). While the ^{12}CO emission shows a comparatively smooth distribution of emission outside of the optical H II regions, the more optically thin ^{13}CO emission shows the presence of several filaments of molecular gas.

4.4. *IC 443*

The ^{12}CO map was extended to the northeast of the Gem OB1 cloud complex to cover the supernova remnant IC 443 near the heart of the Gem OB1 association (see Fig. 1). A contour map of the peak ^{12}CO antenna temperature overlaid

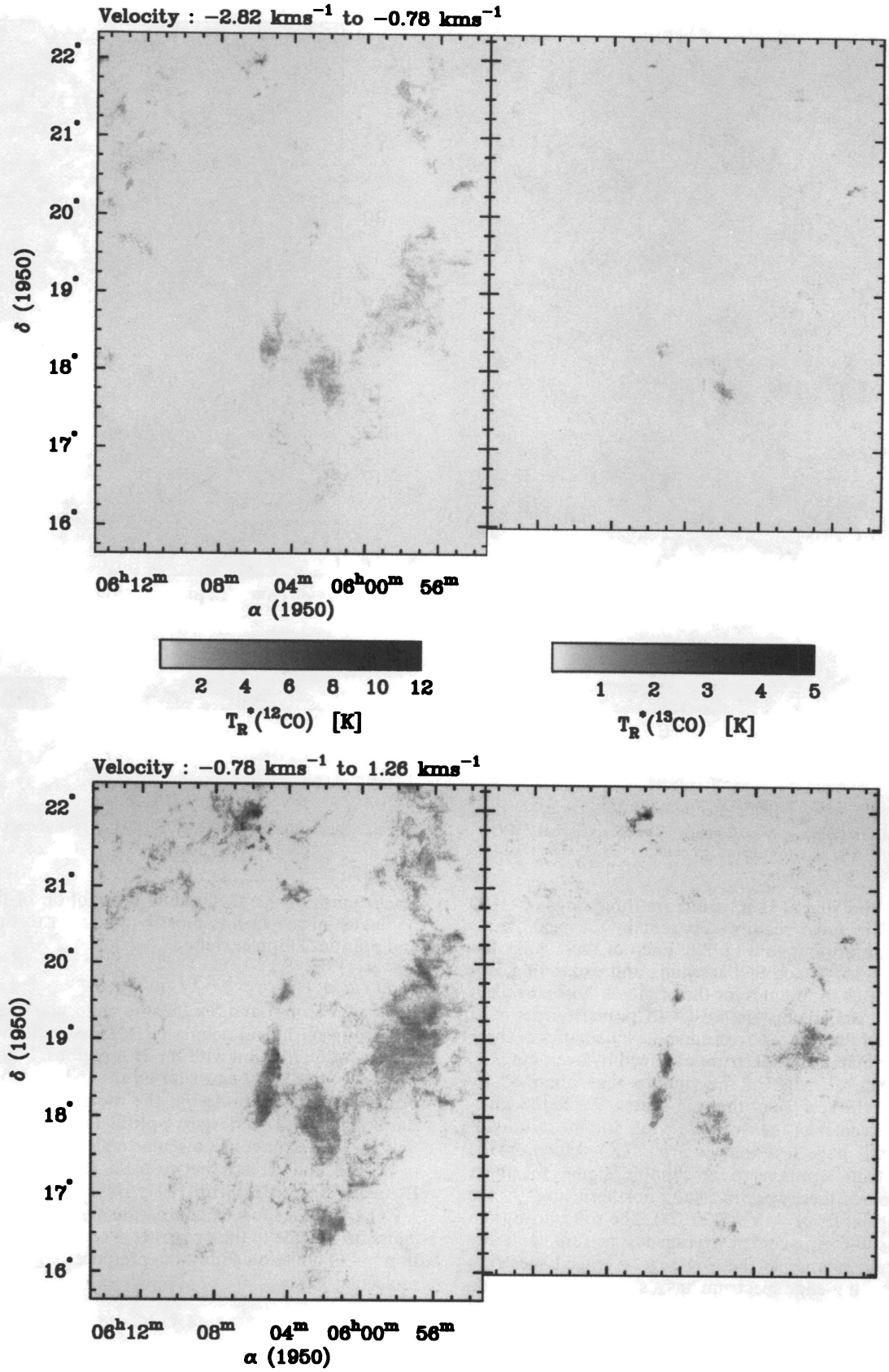

FIG. 3.—Peak antenna temperature maps for the ^{12}CO (*left panels*) and ^{13}CO (*right panels*) averaged over every three channels (2 km s^{-1}) in the spectrometers. The ^{12}CO data were degraded to the velocity resolution of the ^{13}CO data for these images. The gray scale wedges shown in the first velocity image represents the intensity scale for each of the maps.

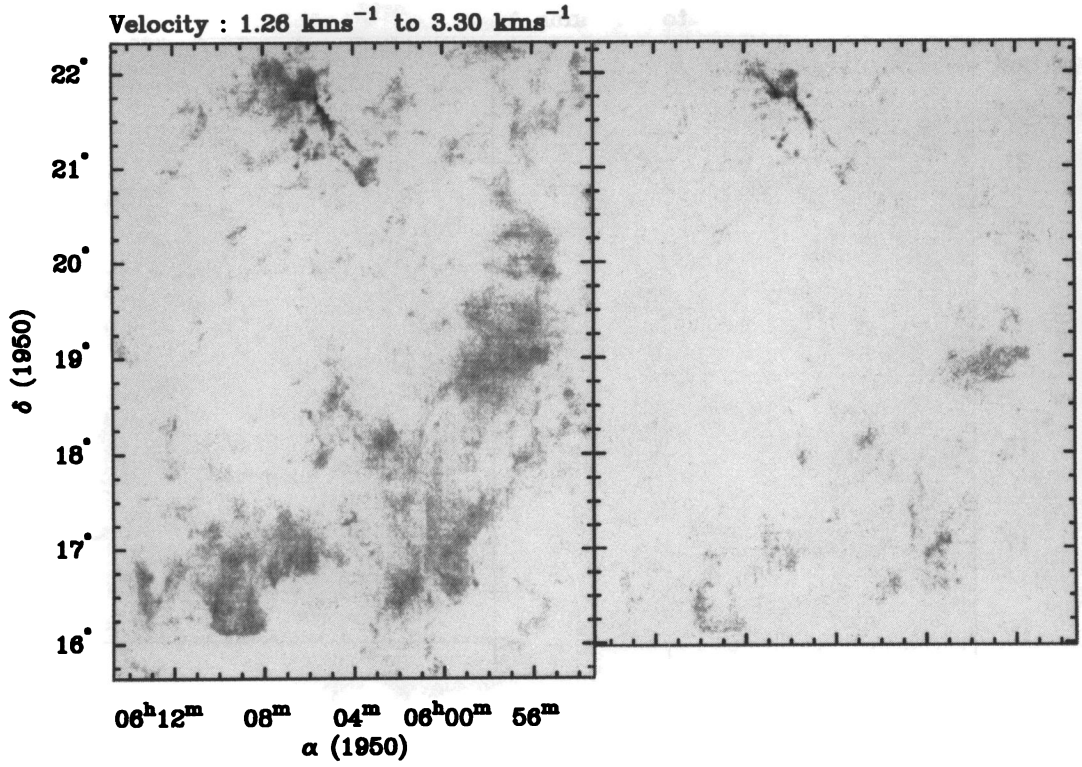

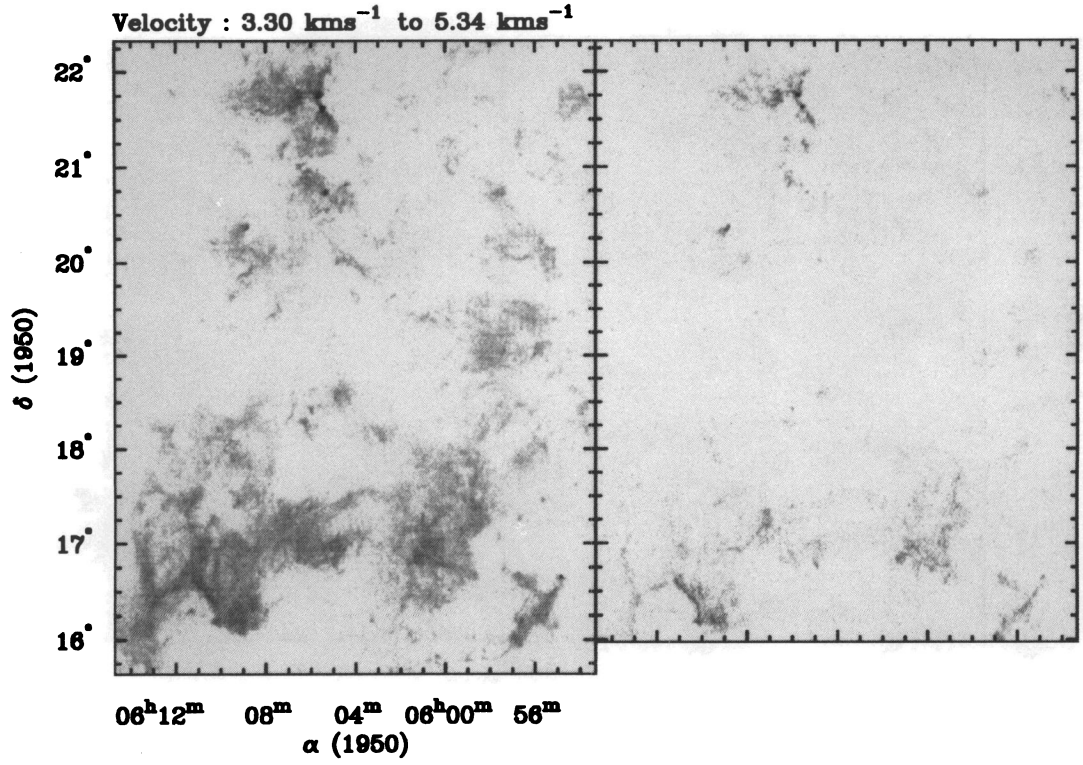

FIG. 3—*Continued*

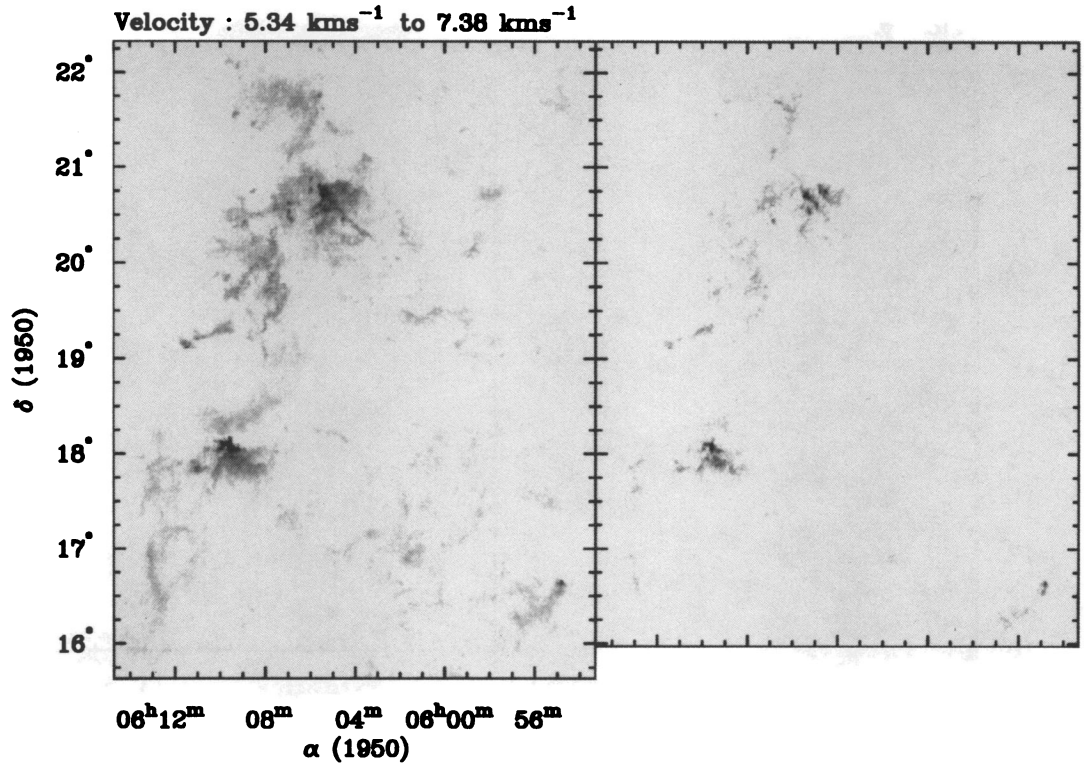

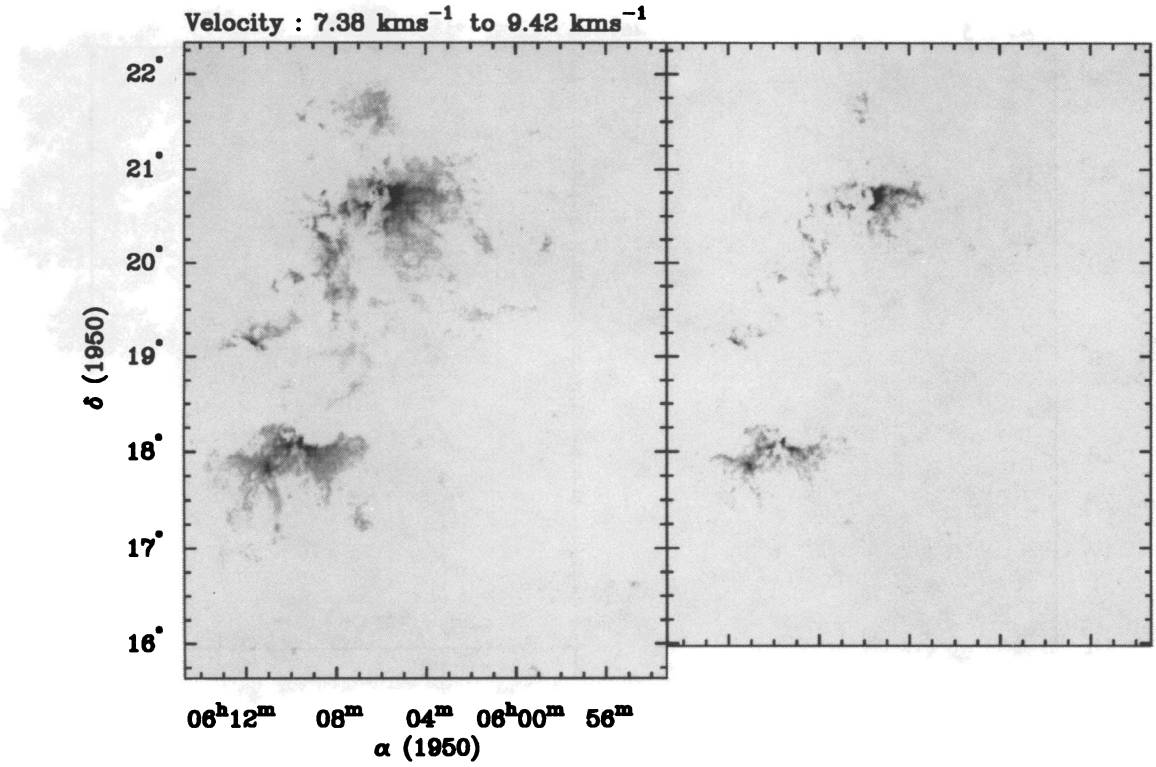

FIG. 3—*Continued*

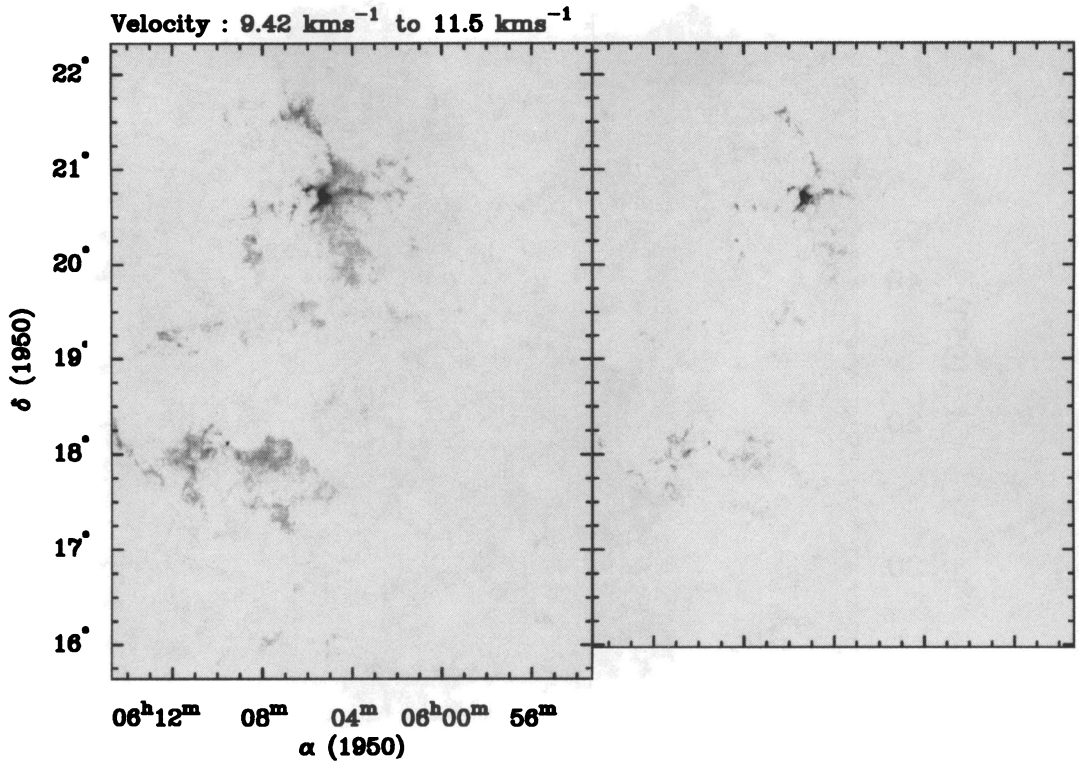

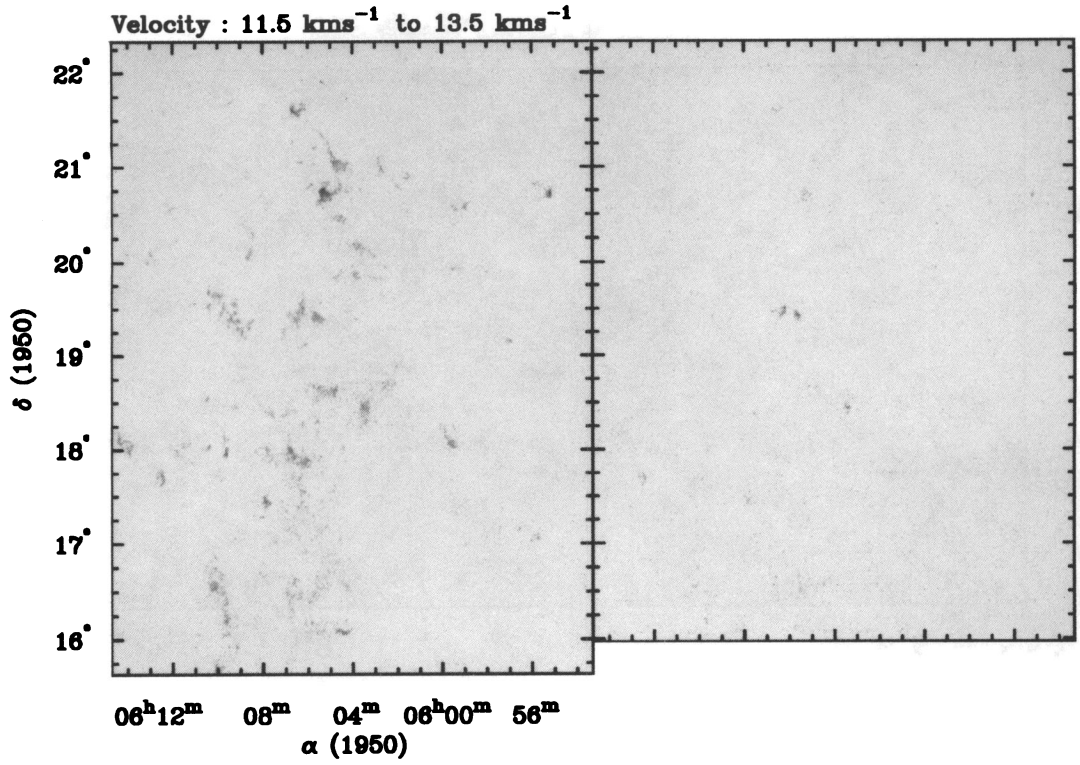

FIG. 3—*Continued*

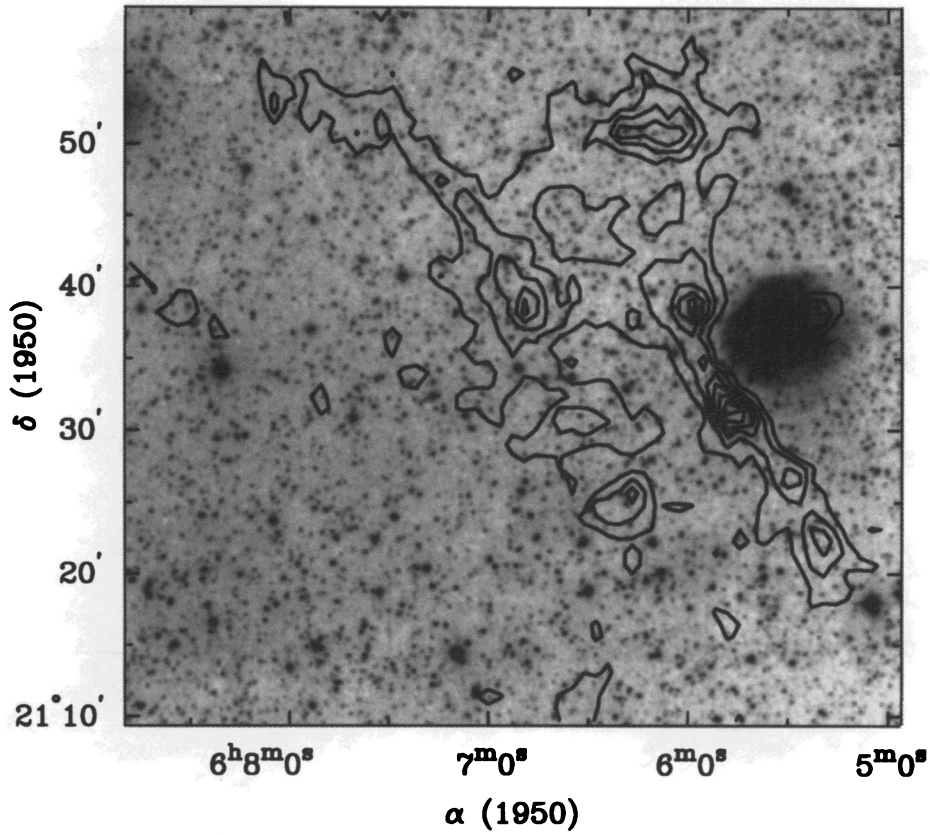

FIG. 4.—Overlay of the ^{13}CO peak antenna temperature on a digitized red Palomar Sky Survey print of the Sh 247 H II region. Contour levels begin at $T_R^* = 1.5$ K with increments of 1.0 K. The velocity images suggest the presence of at least three filaments in this region. One of the filaments wraps along the eastern edge of Sh 247 and contains enhanced column densities and kinetic temperatures, which strongly suggests an association between the H II region and the molecular gas.

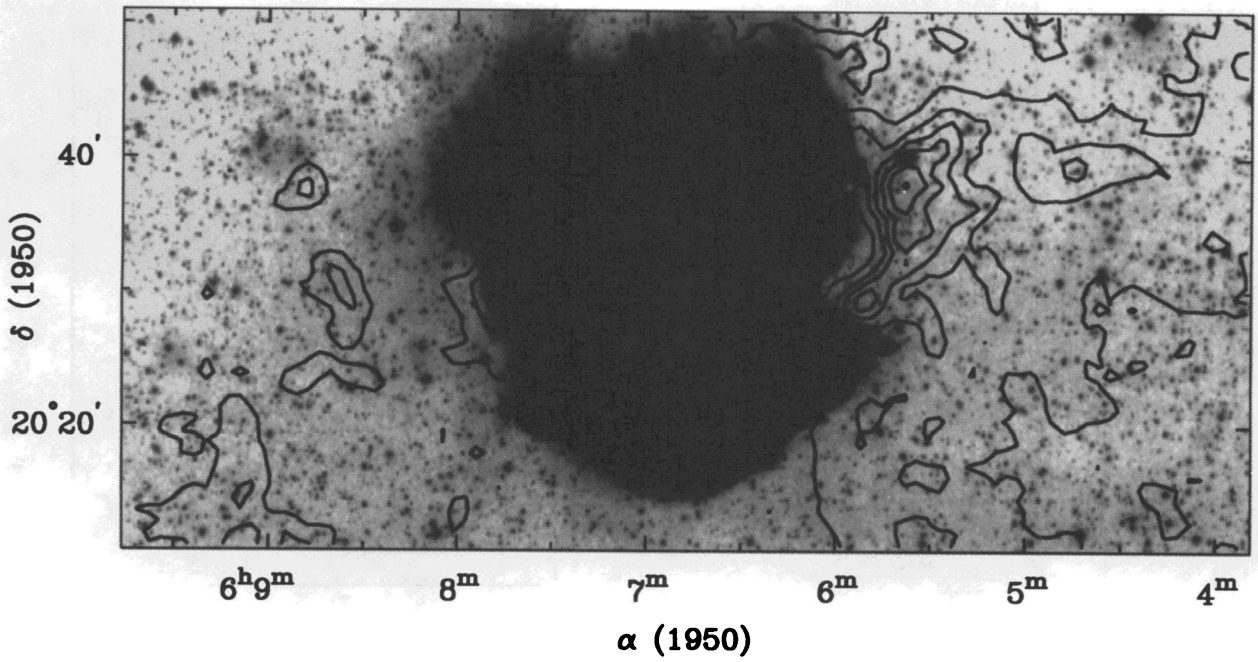

FIG. 5.—Overlay of the ^{13}CO peak antenna temperature on a digitized red Palomar Sky Survey print of the Sh 252 H II region. Contour levels begin at $T_R^* = 1.0$ K with increments of 2.0 K. The morphology suggests that the expanding H II regions or stellar winds have created a cavity in the molecular gas. The size of the cavity and the inferred column densities along the right rim are consistent with this conjecture.

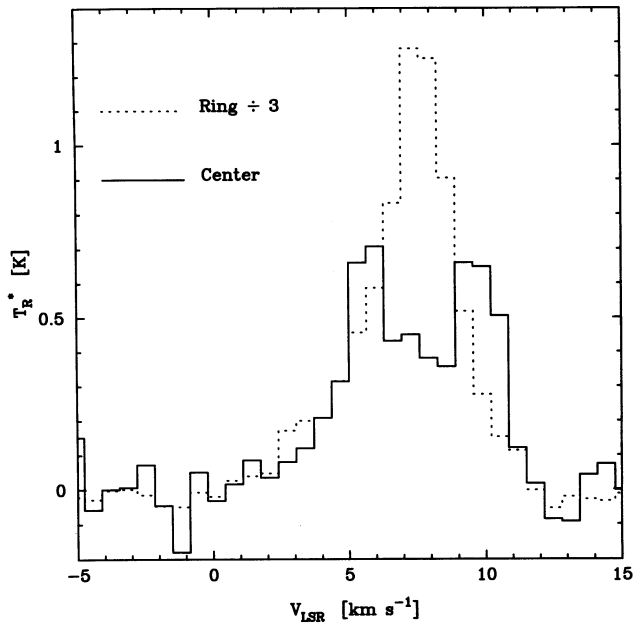

FIG. 6.—Comparison of the average ^{12}CO spectrum toward the center of the ring at (α, δ) = (6^h9^m, 20°20′), with the average spectrum around the edge of the ring. The ring-edge average spectrum has been scaled by $\frac{1}{3}$. The ring-center spectrum shows a double peaked line profile, while the ring-edge averaged spectrum contains a single peak at a velocity midway between these peaks. These observations are consistent with a shell of molecular gas expanding at a velocity of 2.25 km s^{-1}.

on the red Palomar Sky Survey print in shown in Figure 8. Most of the molecular gas runs nearly north-south across the face of the IC 443 supernova remnant. Dickman et al. (1992) speculate that the supernova blast wave is ablating the material off of several clumps, as in some instances, the ^{12}CO lines have velocity extents of up to 80 km s^{-1}. This higher velocity gas extends outside the bandwidth of the 250 kHz spectrometers.

4.5. *BFS 52*

Other features in the Gem OB1 molecular cloud complex also contain kinematic signatures suggestive of expansion. The most spectacular of these is the 1°.5 arc that extends from the southeast corner of the Sh 254–258 region near (α, δ) = (6^h14^m, 18°) at a velocity of ~12 km s^{-1} (see Fig. 3) and connects up to BFS 52 region at (α, δ) = (6^h11^m, 19°). (Note, however, that the filament containing BFS 52 runs across this larger arc.) The centroid velocity of the ^{12}CO emission shifts systematically by ~5 km s^{-1} over the length of the arc. The centroid velocity perpendicular to the arc along this northern extent also changes systematically, with a velocity gradient of ~0.3 km s^{-1} pc^{-1} over a 6 pc length. There is a dearth of ^{12}CO and ^{13}CO emission interior to this arc. Even after averaging 828 ^{12}CO spectra adjacent to the eastern edge of the arc, no emission was detected at a 3 σ RMS level of $T_R^* = 0.07$ K, although ^{12}CO emission was detected near the northern extent of the ring at the 0.15 K level. Thus both the kinematics and spatial distribution of the molecular gas suggest that this feature represents a swept up arc of gas. The curvature of the arc suggests a relationship with the Sh 254–258 group, but since the ^{12}CO emission extends over a much larger area than the optical nebula, this association remains somewhat speculative.

4.6. *Diffuse Emission*

The western and southern edges of the Gem OB1 complex are largely devoid of current massive star formation as traced by optical nebulosity on the Palomar Observatory Sky Survey prints and luminous far-infrared sources in the *IRAS* Point Source Catalog (Version 2, 1988; see Carpenter et al. 1995). The bright rims found along the optical H II regions discussed above are also lacking, as the peak ^{12}CO antenna tem-

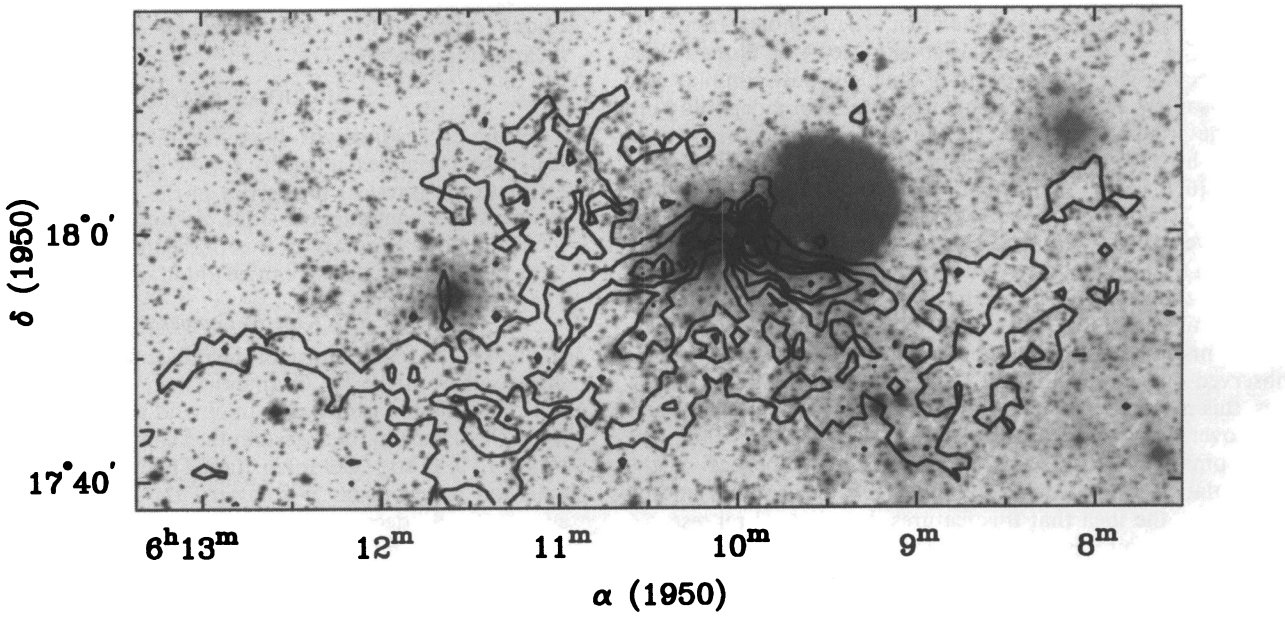

FIG. 7.—Overlay of the ^{13}CO peak antenna temperature on a digitized red Palomar Sky Survey print of the Sh 254–258 region. Contour levels begin at $T_R^* = 1.5$ K with increments of 1.5 K. The molecular gas wraps along the southern edge of Sh 254 (the largest H II region in the group). The brightest molecular emission occurs between the Sh 255 and Sh 257 H II regions. As with Sh 247 and Sh 252 (see Figs. 4 and 5), it appears that the H II regions have had a strong influence on the current structure of the molecular gas.

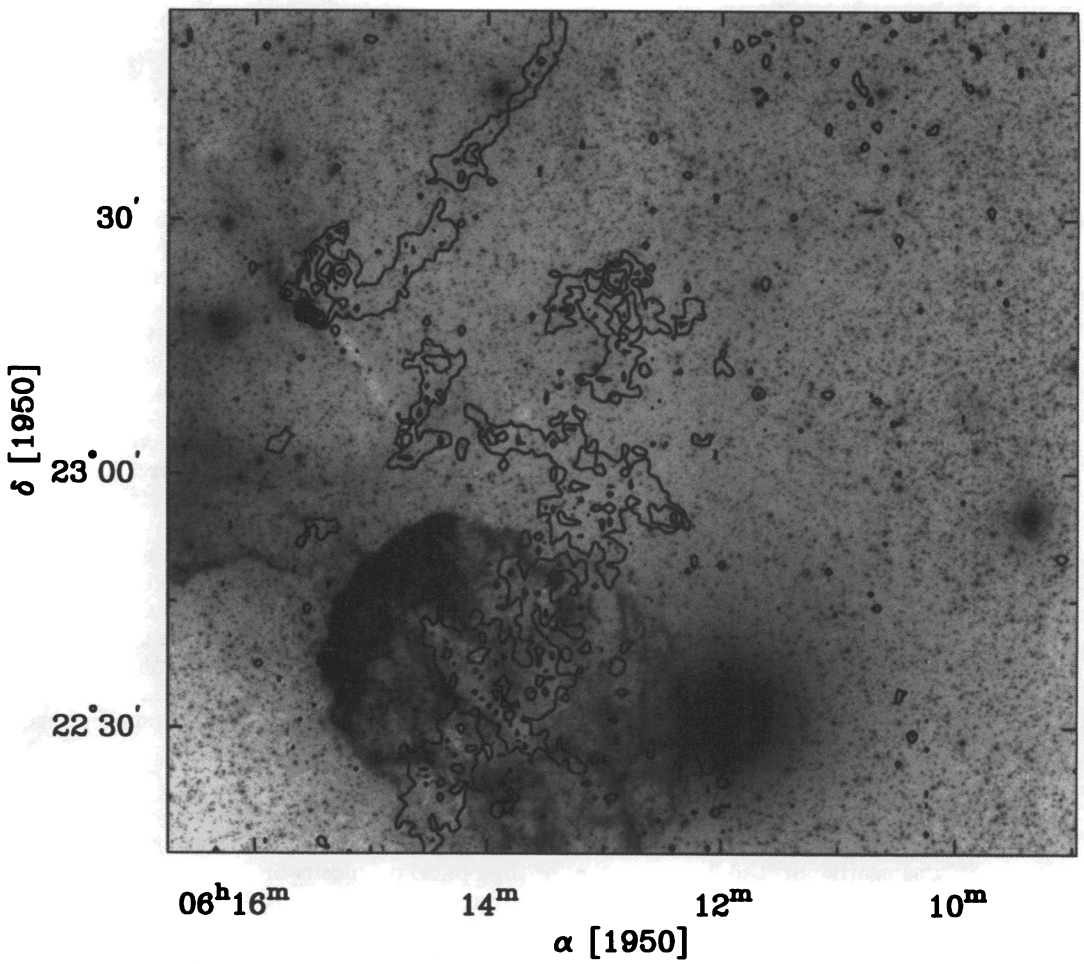

FIG. 8.—Contour map of the peak ^{12}CO antenna temperature toward IC 443 overlaid on the red Palomar Sky Survey print. Contour levels begin at $T_R^* = 2.5$ K with increments of 2.0 K. Note that the high resolution filter backs do not cover the full range of velocities observed previously in this region (Dickman et al. 1992).

peratures in these regions of the Gem OB1 complex are generally $T_R^* \lesssim 4$–5 K (for further discussion, see § 7). Nonetheless, the molecular gas in this region of the Gem OB1 complex also contains a few arc-shaped structures similar in morphology to those described above. The most pronounced of these structures is the semi-circle of ^{12}CO and ^{13}CO emission found near $(\alpha, \delta) = (6^h12^m, 16°)$ that extends for $\sim 0.^\circ5$ (17 pc at a distance of 2 kpc). This sharp boundary in the molecular emission continues westward in this region of the Gem OB1 complex, although the shape of the boundary becomes more irregular.

Along the western edge of the Gem OB1 complex, extended ^{12}CO emission is observed that is largely not detected in ^{13}CO. This emission begins at velocities near -3 km s^{-1}, and is observed out to velocities of ~ 5 km s^{-1}. At the lower velocities, this material appears as an arc-shaped structure that persists over a velocity range of ~ 8 km s^{-1} (13 channels in the spectrometer). As discussed in § 7.2, the properties of the molecular gas along this arc are remarkably similar, lending support to the idea that this features does indeed represent a coherent structure. Furthermore, the curvature of this arc suggests a physical relationship with either Sh 252 or the Gem OB1 association (see § 7.2). Note that while spatial variations in the intensity ^{13}CO are observed toward this "arc" and the emission in the southeast corner of Gem OB1, significant portions of the molecular are *not* necessarily adequately described as "filamentary," and in that respect these regions are distinctly different from the molecular gas around the star-forming regions.

5. METHODS OF ANALYSIS

Before proceeding with the quantitative analysis of the Gem OB1 cloud complex, a brief overview of the procedures used to estimate the physical properties of the molecular gas (kinetic temperatures, column densities, and masses) is provided. A more detailed summary of this procedure, commonly referred to as the "LTE analysis," can be found in Dickman (1978).

5.1. *Kinetic Temperatures*

The kinetic temperature of the molecular gas can be directly measured from the ^{12}CO antenna temperatures by assuming that the emission is optically thick and thermalized. The validity of the optically thick assumption can be estimated from the ratio of ^{12}CO to ^{13}CO intensities. The ratio of ^{12}CO to ^{13}CO emission ranges from 2–5 toward the brightest regions and systematically decreases to $\sim$10–15 toward the low-intensity emission. This intensity ratio is significantly lower than the inferred ^{12}CO to ^{13}CO abundance ratio of 57–74 for the solar neighborhood (Langer & Penzias 1993), and indicates that the ^{12}CO emission is optically thick wherever ^{13}CO is detected. Finally, excitation models that included trapping indicate that the ^{12}CO emission should be close to thermalization wherever ^{13}CO is detected in our maps (Kutner & Leung 1985; Lee et al.

1994). Thus the ^{12}CO peak antenna temperature should be a reasonable probe of the gas kinetic temperature where ^{13}CO is detected.

5.2. *Column Densities and Masses*

For lines of sight with both ^{12}CO and ^{13}CO detections, the ^{13}CO column densities were estimated using the LTE analysis described by Dickman (1978). The ^{13}CO line widths were used in the column density determinations, and were computed by multiplying the second velocity moment (i.e., velocity dispersion) by a factor of 2.35 to convert to a full width at half-maximum, as is appropriate for Gaussian shaped lines. Gaussian line profiles are a reasonable approximation except toward Sh 247, where often two or more distinct features are observed.

Estimating the column densities toward lines of sight without ^{13}CO detections is more difficult since the ^{12}CO emission may still be optically thick. To better determine the ^{12}CO to ^{13}CO ratio toward these regions, the average ^{12}CO and ^{13}CO spectra were obtained toward lines of sight that have a 3 σ or greater ^{12}CO detection (see § 7). The ratio of the ^{12}CO to ^{13}CO integrated intensities toward these regions is 47 ± 8. If ^{12}CO and ^{13}CO both have the same excitation temperature, and the isotopic ratio is 60 (Langer & Penzias 1993), then the average optical of ^{12}CO is ~ 0.5 and the line center optical depth is ~ 3. However, these values represent lower limits to the ^{12}CO optical depth since the ^{12}CO emission could be optically thick and have a higher excitation temperature relative to ^{13}CO due to radiative trapping. To further constrain the possible opacity of the ^{12}CO emission, a large velocity gradient (LVG; Goldreich & Kwan 1974) model was used to determine the physical conditions in which ^{12}CO, but not ^{13}CO, would be detectable. A range of H_2 column densities (10^{20}–10^{21} cm^{-2}) and H_2 volume densities (100–3000 cm^{-3}) were modeled assuming a ^{13}CO to H_2 abundance of 1.5×10^{-6} (Bachiller & Cernicharo 1986), a ^{12}CO to ^{13}CO abundance ratio of 60 (Langer & Penzias 1993), a kinetic temperature of 7 K (Mead & Kutner 1988), and a line width of 2 km s^{-1} (§ 7.2). It should be noted, however, that these properties have been established for regions with strong ^{12}CO (and usually ^{13}CO) emission, and that the molecular gas producing the extended ^{12}CO emission may be substantially different. The results of this analysis indicate that the ^{12}CO opacity could have values as large as 20 at the lower densities and as small as 2 for the higher densities. Thus we expect the ^{12}CO optical depth to be greater than that estimated assuming equal excitation temperatures for ^{12}CO and ^{13}CO. Therefore, to estimate the ^{12}CO column density toward regions with only ^{12}CO emission, we have assumed that the ^{12}CO optical depth is 6, which is midway between the extremes suggested by the models. Based on the LVG models, the lines of sight with only ^{12}CO emission probably have densities of a few hundred cm^{-3} and H_2 column densities of a few $\times 10^{20}$ cm^{-2}.

The ^{13}CO column densities computed from the LTE analysis were converted into H_2 column densities by assuming an ^{13}CO to H_2 abundance of 1.5×10^{-6}, which is an average of the values measured in solar neighborhood molecular clouds (Bachiller & Cernicharo 1986). Similarly, ^{12}CO column densities were converted into H_2 column densities assuming a relative abundance of 0.9×10^{-5}, which comes from assuming a ^{12}CO and ^{13}CO abundance ratio of 60 (Langer & Penzias 1993). Finally, in computing molecular masses, a factor of 1.36 was included to take into account the mass contribution of helium.

6. ENERGETICS AND MODELS OF EXPANDING SHELLS

6.1. H II *Regions*

As argued in § 4, the morphology of the arcs of molecular gas found adjacent to the optical H II regions suggests that these features represent swept up molecular material. To examine this conjecture more quantitatively, in this section we compare theoretical models for the evolution of H II regions with the observed properties of the molecular gas. This analysis is necessarily somewhat simplified since the current models generally do not yet take into account various complexities such as clumpy molecular clouds and the different forces that may be involved (e.g., stellar winds, thermal pressure, the "rocket" effect) at different stages of evolution of the H II region. Nonetheless, it is expected that this analysis will provide a first order indication as to whether the arc shaped structures have likely formed as a result of the dynamical evolution of H II regions.

The expansion of an H II region is first caused by the pressure gradient between the hot, dense ionized gas in the initial Stromgren sphere and the surrounding cold molecular material. This expansion proceeds supersonically and drives a shock front that sweeps up a spherical shell of molecular gas (Spitzer 1978). At the same time, a stellar wind from the ionizing star also contributes to the expansion of the molecular shell as well (Castor, McCray, & Weaver 1975; Weaver et al. 1977). For the purpose of this discussion, the H II region eventually breaks out along one edge of the molecular cloud, creating a "champagne" flow (Tenorio-Tagle 1979) of ionized gas. This decreases the electron density in the H II region and diminishes the contribution of thermal pressure to the further expansion of the H II region. Instead, the flux of ultraviolet photons impinging on the swept up shell increases due to the decreased electron density, which imparts additional momentum to the shell through the "rocket" effect (Spitzer 1978). The rocket effect can lead to a substantial increase in the expansion velocity of the shell provided that no additional molecular material is accumulated in the swept up shell (Bally & Scoville 1980).

This general picture of the evolution of H II regions leads to specific predictions concerning the size and expansion velocity of the swept up shell, and the amount of matter accumulated by the shock front. To examine the observed properties of the molecular gas surrounding the optical H II regions, Figure 9 shows the azimuthal average of the radial variations of the kinetic temperatures, H_2 column densities, and ^{13}CO line widths. For Sh 247 and Sh 254, a radial distance of 0.0 pc in Figure 9 corresponds to the center of the optical H II region, while for Sh 252, the adopted center position is not coincident with the exciting star for Sh 252, but instead was chosen to be the center of curvature implied by the bright arc of emission on the western edge of the H II region. This position was chosen to prevent smearing the properties of the ridge in radius. Furthermore, the molecular gas properties were only calculated within the position angles where the molecular gas actually outlines the H II region, since the specific interest is to study the properties of molecular gas around apparently ionization bounded H II regions.

The most marked change in the gas properties at the H II region–molecular cloud interface is the order of magnitude

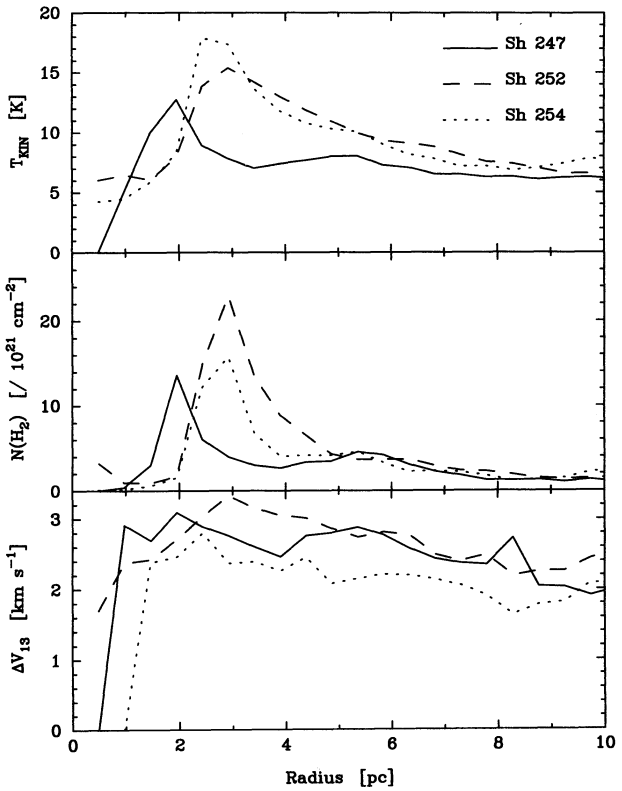

FIG. 9.—Variation in the kinetic temperature, H_2 column density, and ^{13}CO line width (FWHM) across the bright rims around the optical H II regions Sh 247, Sh 252, and Sh 254. The interfaces of the H II regions with the molecular gas all show a marked increase in the column densities and kinetic temperatures.

increase in the H_2 column density as compared to the ambient molecular material. In fact, the highest H_2 column densities in the Gem OB1 complex are found along these interfaces. The kinetic temperature typically shows a enhancement of a factor of 2–3, and the line widths increase only marginally. These latter two properties peak at approximately the same radial length as the corresponding column density distributions, although they exhibit a more gradual decline with radius into the cloud. The increased temperature of the molecular gas most likely reflects a combination of heating from the associated H II region and possibly from embedded stars within these bright rims (Carpenter et al. 1995). Systematic changes in the centroid velocity across the interfaces that might be indicative of expansion were also searched for, but no such gradients were found, as only random fluctuations in the velocity of the emission on order of 1–2 km s^{-1} emission were observed.

The Sh 252 affords the best comparison to the theoretical models since the region has been frequently studied and therefore contains the necessary supplemental information. The exciting star for Sh 252 is an O6.5 V star with an inferred age of 2 Myr from the associated cluster (Grasdalen & Carrasco 1975). Such a star is expected to have a Lyman continuum flux of $10^{49.0}$ s^{-1} (Panagia 1973) and a stellar wind power of $\sim 10^{36}$ ergs s^{-1} (Abbott 1982). The observed angular size of the H II region is $\sim 30' \times 25'$, corresponding to a linear size scale of 17 × 15 pc. The projected distance between the ionizing star and the bright rim is ~8.4 pc.

To make the appropriate comparisons between the observations and the models, the evolutionary stage of the H II regions in the schematic outlined above needs to be identified. Molecular material does not completely surround any of the H II regions considered here, implying that these H II regions were ionization bounded only in the early stages of their evolution, and that thermal pressure from the hot, ionized gas may not be as important in the current evolution of the expanding H_2 region as it was in the past. Patel et al. (1995) modeled the kinematics of an H II region ionized by an O6 star, similar to that for Sh 252, by considering thermal pressure in the early stages for the H II region and the rocket effect once breakout is achieved (see also Mazurek 1980; Maddalena & Morris 1987). In this model, the expansion velocity of the shell driven by thermal expansion rapidly decelerates as matter is swept up. Assuming an initial density of 1000 cm^{-3}, by 2 Myr the expansion velocity has decreased to ~1.5 km s^{-1}, and the expected size of the H II region of this age is 7 pc. After breakout, where the H II region is depressurized, the swept up shell of molecular gas will continue to decelerate as long as new material is swept up by the shell (Bally & Scoville 1980). We believe that the H II regions are in this phase of evolution since there appears to be material still remaining to be swept up, which is consistent with the observed low expansion velocities of the molecular gas. Furthermore, the total mass of material within the bright rim surrounding Sh 252, estimated to be $\sim 1.4 \times 10^4\ M_\odot$ using the LTE analysis on the ^{12}CO and ^{13}CO data, agrees well with the amount of molecular gas expected to have been swept up ($1.2 \times 10^4\ M_\odot$) assuming that the interior of the shell was once uniformly filled with molecular gas with a column density equal to that observed outside the shell (Fig. 9; see also Lada & Wooden 1979). Thus for Sh 252, the size of the H II region, the amount of molecular gas in the bright rim, and the expansion velocity of the bright rim is consistent with a 2 Myr old H II region that is ionizing dense molecular material.

The age estimates for the other optical H II regions are not available, but since the models are only weakly dependent on the age of the massive star, we compare the data with the models assuming an age of 2 Myr. For Sh 247 and Sh 254, respectively, the observed radii of the H II regions are 1.0 and 1.6 pc, respectively. The main exciting stars for both nebula are B0 V stars (Hunter & Massey 1990). The expected sizes of the H II regions for an assumed H_2 density of 10^3 cm^{-3} are 1.6 and 1.8 pc. The observed mass within the arc bordering Sh 254 is within a factor of 2 of the expected mass based on the observed column density distant from the H II region, while the observed mass for Sh 247 is a factor of four less than the expected mass. Thus the properties of the arc of molecular gas around Sh 254 is consistent with it being swept up molecular material. The arc of molecular gas around Sh 247 is smaller and contains more mass than predicted from the model. This may merely indicate that the ambient density was higher than assumed. For example, an initial density of 4×10^3 cm^{-3}, for example, would make the observations more consistent with these models.

The salient result of this analysis is that the morphology and properties of the bright rims surrounding the extended optical H II regions are generally consistent with the notion that these features represent swept up molecular material. While little kinematic evidence is present to suggest that this is the case, simple models for the expansion of H II regions suggests that the expected expansion velocity is of order 1–2 km s^{-1} and would be difficult to detect, especially given that these bright rims are observed nearly edge on.

6.2. *Arcs and Rings*

As discussed in § 4, that while the other arc-shaped structures in Gem OB1 do not have obvious optical counterparts, the morphology and in some instances kinematics also suggest that these features represent expanding shells and rings of molecular material. It should be emphasized, however, that rarely are the approaching and receding parts of the shell actually observed, with the shell described in Figure 6 being the lone exception. While emission is detected in the average ^{12}CO spectra toward the center of other rings, the emission has a single velocity component, which in a couple of cases differs by up to 1–2 km s^{-1} from the velocity of the ^{12}CO emission found along the perimeter of the ring. It is not clear if this velocity difference represents the expansion of one hemisphere of a shell, or merely the random velocity fluctuations in the molecular gas. Regardless, unless the ^{12}CO emission is optically thin through the center of the ring, a disk of emission of nearly uniform antenna temperature should be observed since limb brightening will not occur in an optically thick tracer. To determine if the observed rings could represent limb brightened shells, a LVG radiative transfer model was used to determine the predicted ^{12}CO and ^{13}CO antenna temperatures for shells of various volume densities and thicknesses. Under no conditions could the observed variations in the ^{12}CO and ^{13}CO antenna temperatures and the observed shell masses be produced assuming standard molecular abundance ratios and kinetic temperatures.

One possible solution is that the molecular cloud was initially oblate and not spherical. Therefore, when the expansion of the H II region or stellar wind blown bubble breaks out on the short axis of the cloud, the other two sides will continue to sweep up molecular material, which can lead to ring like structure. Maddalena & Morris (1987) proposed such a scenario for the ring of clumps found around λ Ori. If molecular clouds are indeed oblate, the observed rings places a constraint the thickness of the cloud. The three rings near Sh 252, for example (see § 4), places a conservative upper limit to the cloud thickness of $\sim$15 pc (i.e., the diameter of the rings). The molecular gas in this region extends for $\sim$1°, implying a lower limit to the major to minor axis ratio of $\sim$4.

The kinetic energies of these structures can potentially place constraints on the phenomena that produced them. The ring near Sh 252 (see Fig. 6) with an expansion velocity of 2.3 km s^{-1} has a mass of $\sim 2 \times 10^3\ M_\odot$ and a dynamical time scale of 2 Myr, which implies a kinetic energy of 3×10^{47} ergs and a mechanical power of 5×10^{33} ergs s^{-1}. One possible mechanism consistent with this energy requirement and that will naturally produce the expansion motions observed toward this ring and account for spherical shape of the molecular gas is stellar winds from a late to early B type star (Bally & Lada 1983). The other two large rings near Sh 252 have kinetic energies of ~ 5–10×10^{46} ergs for an assumed expansion velocity of 2 km s^{-1}. Similarly, the large loop running from BFS 52 down to Sh 254–258 has a mass of $\sim 2.7 \times 10^3\ M_\odot$ and an estimated expansion velocity of $\sim$3 km s^{-1} from the observed velocity gradient, implying a kinetic energy of 2×10^{47} ergs. The important result from this analysis is that the kinetic energies for these structures are not formidable, and can be supplied by stellar winds from moderate mass stars.

7. PHYSICAL PROPERTIES OF THE GEMINI OB1 CLOUD COMPLEX

While the global properties of giant molecular cloud complexes have been well documented, the high-resolution, well sampled maps presented here offer unique opportunities to study how the properties of the molecular gas vary throughout a single cloud complex since many of the large scale structures are clearly resolved. The properties of the molecular gas will be characterized for the Gem OB1 complex as a whole and for seven designated subregions within the Gem OB1 complex. The subregions were selected as regions with extended, bright ^{13}CO emission (i.e., high H_2 column density) and are not intended to be a break down of the Gem OB1 complex into individual "clouds." It is hoped, however, that this segregation will enable the properties of the molecular gas to be contrasted within different regions of the Gem OB1 complex. Table 1 summarizes the location and sizes of the designated subregions. These subregions differ dramatically in terms of their star formation characteristics. Subregions 1, 2, and 3 are each associated with optical H II regions, and of the remaining four subregions, only subregion 6 contains an optically recognizable star forming region, the Herbig Ae/Be star HD 250550.

7.1. *Luminosities, Masses, and Volume Densities*

Inspection of the ^{12}CO and ^{13}CO images shown in Figures 2*a* and 2*b* indicates that much of the projected surface area of the Gem OB1 complex is detected in ^{12}CO but not ^{13}CO. While the distinction between regions with and without ^{13}CO emission is based on the noise characteristics of the map and is therefore somewhat arbitrary, it nonetheless serves as a useful division to evaluate the origin of the ^{12}CO luminosity in the Gem OB1 cloud complex. Therefore, average ^{12}CO and ^{13}CO spectra were constructed for three cases based on the detectability of the ^{12}CO and ^{13}CO emission: (a) lines of sight with both ^{12}CO and ^{13}CO detections (at the 3 σ noise level), (b) those with ^{12}CO detections only, and (c) those with no ^{12}CO and ^{13}CO detections. Figure 10 contains the average spectra for each of these cases, which shows that ^{12}CO emission is

TABLE 1

SUBREGIONS WITHIN GEMINI OB1

REGION	α (1950)	δ (1950)	MAP SIZE ($\alpha \times \delta$)		V_{LSR} (km s^{-1})	COMMENTS
				(pc)		
1.....	6^{h}06^{m}55^s	21°39′43″	63′ × 55′	37 × 32	3.8	Sh 247
2.....	6 05 54	20 28 34	68 × 47	39 × 27	7.2	Sh 252
3.....	6 10 18	17 47 27	93 × 59	53 × 34	6.8	Sh 254–258
4.....	5 57 41	18 50 13	68 × 43	39 × 14	1.2	
5.....	6 02 58	17 51 38	34 × 43	20 × 25	0.5	
6.....	6 00 10	16 50 57	63 × 63	37 × 37	3.0	HD 250550
7.....	6 10 00	16 18 18	51 × 45	30 × 26	3.4	

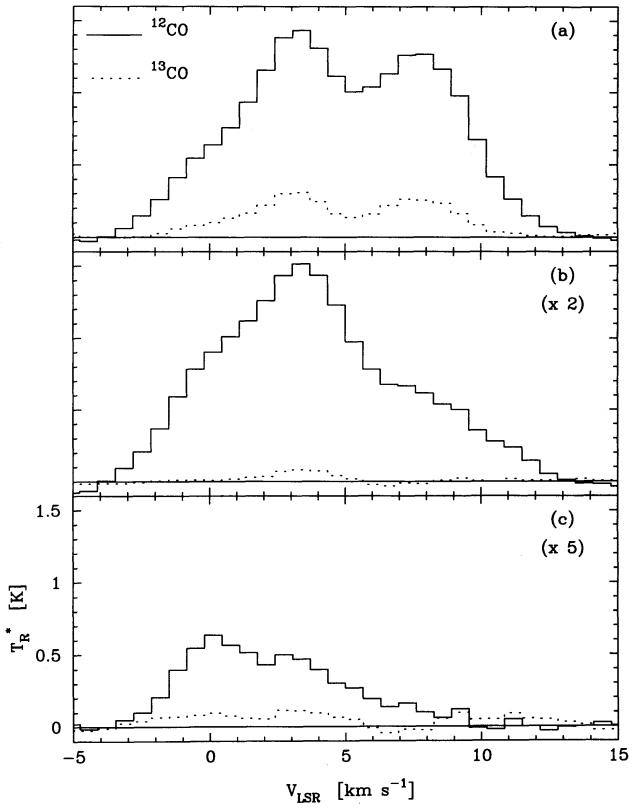

FIG. 10.—Average ^{12}CO (*solid curves*) and ^{13}CO (*dotted curves*) spectra toward lines of sight with both ^{12}CO and ^{13}CO detections at or above the 3 σ noise level (case a), lines of sight with only ^{12}CO detections (case b), and lines of sight with neither ^{12}CO nor ^{13}CO detections (case c). The intensity scale shown for case c is applicables for all three panels. The spectra for cases b and c have been scaled by a factor of 2 and 5, respectively. Of the total ^{12}CO(J = 1–0) luminosity of 1.7×10^5 K km s^{-1} pc^2, 50% originates in lines of sight with only ^{12}CO detections (case b).

clearly present on average in all three cases, and ^{13}CO is detected in cases a and b, but not in case c to within the noise. The total ^{12}CO(J = 1–0) luminosity in the Gem OB1 complex is 1.7×10^5 K km s^{-1} pc^2, of which 41% is contained in case a, 50% in case b, and 9% in case c. The global ^{12}CO to ^{13}CO luminosity ratio is 10.0, and for cases a, b, and c, the ratio is 5.5, 47, and more than 6.0, respectively. The ^{12}CO luminosities and the ^{12}CO to ^{13}CO luminosities ratios for the individual subregions are provided in columns (2) and (3) of Table 2.

This analysis indicates that nearly 60% of the ^{12}CO luminosity from the Gem OB1 cloud complex originates from lines of sight that do not have detectable ^{13}CO emission. Not only is the ^{13}CO weak toward these lines of sight, but its relative strength to ^{12}CO is lower than other regions of the cloud complex. The variation in the ^{12}CO to ^{13}CO ratio is also manifested in the small scale structure of the cloud complex. Toward the brightest ^{12}CO emission regions (which tend to be also high in column density, as discussed in § 7.2), the ^{12}CO to ^{13}CO ratio is ~2–5 and systematically increases toward the lower intensity (column density) regions. In fact, Figure 10 suggests that the ratio on average may be as high as 47 ± 8 in lines of sight detected only in ^{12}CO. The variation in the ^{12}CO to ^{13}CO ratio might be caused by a decrease in the excitation temperature of ^{13}CO relative to ^{12}CO, and/or a decrease in the ^{13}CO opacity if ^{12}CO is still optically thick.

These properties of the ^{12}CO and ^{13}CO emission in the Gem OB1 complex are consistent with what has been observed in other molecular clouds. Cernicharo & Guélin (1987) found strong variations of the ^{12}CO to ^{13}CO intensity ratio as a function of column density in Heiles Cloud 2, with the ratio being as high as 25 toward lines of sight with visual extinctions of ~1 magnitude. Polk et al. (1988) also found systematic variations in the ^{12}CO to ^{13}CO intensity ratios in analysis of molecular emission in the inner Galaxy. The global average ratio found in this study was 6.7 ± 0.7, which is comparable to the subregions but lower than the ratio of 10 for the Gem OB1 complex as a whole (see Table 2). Similarly, Lee, Snell, & Dickman (1990) found a luminosity ratio of 5.5 toward a 3° × 3° region centered on (l, b) = (24°, 0°). As suggested by these studies and confirmed by this analysis of the Gem OB1 cloud complex, the observed ratios of ^{12}CO to ^{13}CO luminosities suggests that the low column density molecular material contribute a significant fraction of the total ^{12}CO luminosity in the interstellar medium (see also Chiar et al. 1994). While the observed ratios in the inner Galaxy are lower than observed for the Gem OB1 complex as a whole, it is not clear if this represents an intrinsic difference between molecular gas in the inner and outer Galaxy or merely that these regions studied by Polk et al. (1988) and Lee et al. (1990) happened to have large quantities of high column density molecular gas.

The LTE masses of the subregions and the Gem OB1 complex are listed in column (4) of Table 2. The masses of the

TABLE 2

MOLECULAR PROPERTIES OF GEMINI OB1

Subregion (1)	L_{12} (2)	L_{12}/L_{13} (3)	M_{LTE} (4)	$\overline{n(H_2)}$ (5)	$\overline{N(H_2)}$ (6)	$N(H_2)_{1/2}$ (7)	f_{22} (8)	σ_{12} (9)	σ_{13} (10)	σ_C (11)	γ (12)
1	1.3×10^4	7.2	3.5×10^4	109	2.1	4.2	21	2.3	1.2	1.9	1.8
2	1.7×10^4	6.5	5.2×10^4	120	2.7	6.3	37	1.7	1.1	0.7	0.5
3	1.6×10^4	7.1	4.3×10^4	74	1.6	3.1	14	1.6	0.9	1.2	0.9
4	8.5×10^3	8.4	2.1×10^4	87	1.3	2.3	2	1.8	1.2	0.9	1.3
5	4.4×10^3	9.3	1.0×10^4	118	1.2	1.9	0	1.9	1.0	1.3	2.8
6	9.8×10^3	10.3	2.1×10^4	65	1.0	1.5	1	1.4	0.8	1.0	1.5
7	5.7×10^3	7.8	1.3×10^4	74	1.1	1.8	0	1.1	0.8	0.9	1.4
Gem OB1.....	1.7×10^5	10.0	3.2×10^5	1.2	1.0	1.8	10	1.7	1.0	3.0	1.9

NOTES.—Col. (1)—Designated subregion; col. (2)—^{12}CO(J = 1–0) luminosity in K km s^{-1} pc^2; col. (3)—ratio of ^{12}CO to ^{13}CO luminosity; col. (4)—LTE mass in $M_\odot$; includes a factor of 1.36 for helium; col. (5)—average molecular hydrogen density in cm^{-3}; col. (6)—average H_2 column density in 10^{21} cm^{-2}; col. (7)—50% point in cumulative $N(H_2)$ distribution in 10^{21} cm^{-2}; col. (8)—percent fraction of mass contained in $N(H_2) \geq 10^{22}$ cm^{-2}; col. (9)—average ^{12}CO velocity dispersion in km s^{-1}; col. (10)—average ^{13}CO velocity dispersion in km s^{-1}; col. (11)—centroid velocity dispersion in km s^{-1}; col. (12)—$\gamma = -2T/W$.

subregions range between $1.0 \times 10^4\ M_\odot$ and $5.2 \times 10^4\ M_\odot$, and the mass for the entire Gem OB1 complex is $3.2 \times 10^5\ M_\odot$. Lines of sight with only ^{12}CO detections, which contribute 50% to the total ^{12}CO luminosity from the Gem OB1 complex, contain 19% of the mass. The designated subregions contain 61% of the mass of the Gem OB1 complex, with the three subregions with on-going massive star formation containing 41% of the total molecular mass. The subregions with massive star formation contain 3–5 times the molecular mass of regions without massive star formation.

The total masses derived from the ^{12}CO and ^{13}CO data may underestimate the total molecular gas mass of the Gem OB1 complex. Comparisons between visual extinction and ^{12}CO and ^{13}CO intensities indicates that these molecules begin to show emission only at a visual extinction threshold of $\sim$0.5–1.6 magnitudes (see compilation by Lee, Snell, & Dickman 1991). Quite plausibly, this extinction threshold may represent the minimum column densities needed to self-shield ^{12}CO and ^{13}CO from photodissociation (van Dishoeck & Black 1988). In comparison, the self-shielding optical depth for molecular hydrogen is $\lesssim$0.1 magnitudes for H_2 densities of 10^3 cm^{-3} (van Dishoeck & Black 1988). As the density decreases, the threshold extinction level increases. Thus molecular hydrogen could exist where ^{12}CO does not. If all the lines of sight with at least a 5 σ ^{12}CO detections do indeed have a threshold extinction level of 1 magnitude which is primarily molecular hydrogen, then the total additional molecular mass to the Gem OB1 complex may be as large as $3 \times 10^5\ M_\odot$, which is comparable of the mass estimated from the ^{12}CO and ^{13}CO observations.

The average density of the molecular material was estimated using the computed LTE masses and an estimated size of the emitting region, and assuming that the material is spherically distributed. The size of the emitted region was defined as the radius of a circle that equals the projected area of the lines of sight with at least a 5 σ ^{13}CO detection, and as such the size is not as sensitive to the chosen box size. The average densities for the subregions computed in this manner, listed in column (5) of Table 2, range between 65 and 120 cm^{-3}, which are typical of the volume densities derived in other nearby molecular clouds (Blitz 1978). No obvious trend is present between the average density and the presence of massive star formation. As shown by Carpenter et al. (1995), however, the subregions with massive star formation have detectable CS(J = 2–1) emission, a signature of dense molecular material, but these regions occupy a small fraction of the total surface area and mass. These average densities are more than an order of magnitude below the ^{13}CO critical density (4000 cm^{-3}; Spitzer 1978), however, these densities are only slightly below the minimum density of $\sim$300 cm^{-3} (for an H_2 column density of 3×10^{21} cm^{-2}) needed to produce detectable ^{13}CO emission. Thus the volume filling factor of the molecular gas is $\lesssim$0.5. The average density for the Gem OB1 complex, computed using the total mass of $3.2 \times 10^5\ M_\odot$ and a radius of 100 pc (i.e., the size of the map) is 1.2 cm^{-3}, thus implying a volume filling factor for the entire complex of $\sim$0.004. This low volume filling factor is as expected since a large fraction of the Gem OB1 complex is devoid of ^{12}CO and ^{13}CO emission (see Figs. 2*a* and 2*b*). In fact, only 50% of the lines of sight observed in ^{12}CO have an integrated intensity at or above the 3 σ noise level. Interestingly, this average proton density of 2.4 cm^{-3} is only $\sim$2 times the global average space density of atomic hydrogen (1.2 cm^{-3}; Spitzer 1978) in the interstellar medium. Furthermore, if the amount of atomic hydrogen in the Gem OB1 complex is comparable to that of molecular hydrogen (see Blitz 1991), the total proton volume density in the Gem OB1 complex is $\sim$4 times that of the global average H I density in the Galaxy. This suggests that the formation of the Gem OB1 complex did not require the conglomeration of excessive amounts of atomic hydrogen above the average galactic H I density.

Finally, we briefly investigate the use of the ^{12}CO luminosity as a tracer of molecular hydrogen mass. Such a relationship has been found based on comparisons of γ ray, ^{12}CO, and H I emission (see review by Bloemen 1989), although why such a relationship should exist is still somewhat of a puzzle given that ^{12}CO is optically thick and a priori should not be an effective mass tracer (see, however, Dickman, Snell, & Schloerb 1986). Table 2 indeed shows that ratio of molecular mass to ^{12}CO luminosity for the subregions varies by less than a factor of 2 between 2.1 and 3.1 $M_\odot$ (K km s^{-1} pc^2)$^{-1}$, with a tendency for the regions without massive star formation to have a slightly lower mass to luminosity ratio.

7.2. *Kinetic Temperatures, Column Densities, and Line Widths*

The distribution of kinetic temperatures are shown in Figure 11, which displays histograms of the kinetic temperatures for the Gem OB1 complex and the seven subregions listed in Table 1. Most lines of sight in each of the subregions have excitation temperatures between $\sim$6–8 K. While the frequency distribution of low kinetic temperatures is uncertain due to requiring at least a 5 σ ^{13}CO detection, the lack of high kinetic temperature lines of sight suggests the bulk of the molecular gas is relatively cold even after allowing for reasonable levels of subthermal excitation (Lee et al. 1994). In subregions 4–7, which contain no massive star formation, the gas kinetic temperature is $\sim$6–8 K, and there is little evidence to suggest that substantial amounts of molecular gas with kinetic temperatures greater than 10 K exists. These excitation temperatures are consistent with those inferred in other molecular clouds at similar galactic radii (Mead & Kutner 1988; Lee et al. 1994), and with the kinetic temperatures expected for gas heating by cosmic rays (Lee et al. 1994). The regions with excitation temperatures in excess of $\sim$10 K are peculiar to subregions 1–3, and these regions must contain additional heating sources for the molecular gas. Undoubtedly the enhanced kinetic temperatures is due to heating from the OB stars and embedded star-forming regions (Carpenter et al. 1995).

The column density distributions exhibit a similar spatial distribution as the kinetic temperatures in the high column density lines of sight are preferentially in the subregions forming massive stars. Figure 12 shows the fractional H_2 mass in a subregion as a function of column density. Various statistical properties are summarized in Table 2 that characterize the data shown in Figure 12; these include the average column density toward lines of sight with at least a 5 σ ^{12}CO detection (col. [6]), the column density representing the 50% level in the cumulative mass distribution (col. [7]), and the fraction, f_{22}, of the total mass contained in lines of sight with $N(H_2) \geq 10^{22}$ cm^{-2} (col. [8]). The estimated column densities toward lines of sight with at least a 5 σ ^{12}CO detection range from 1.3×10^{20} cm^{-2} to 6.4×10^{22} cm^{-2} averaged over a 50″ region. The four subregions (4–7) without massive star formation have average column densities of 1.0–1.3 $\times 10^{21}$ cm^{-2}. Very few lines of sight have column densities in excess of 10^{22} cm^{-2} in these four subregions, as at least 98% of the mass are contained in relatively low column density gas. In contrast, the three subregions

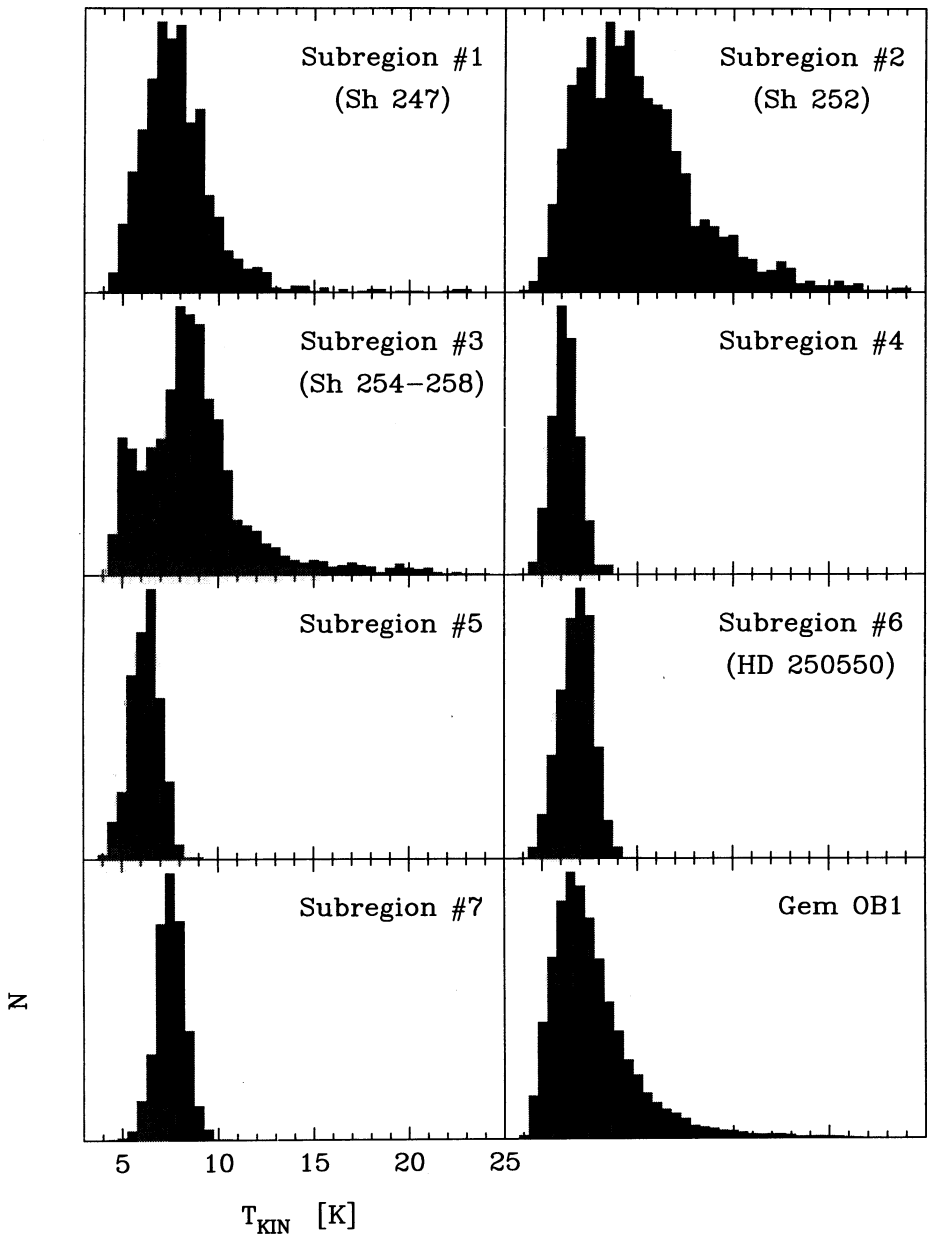

FIG. 11.—Frequency distribution of the molecular gas kinetic temperature in the seven designated subregions and the Gem OB1 complex has a whole toward lines of sight with at least 5 σ ^{13}CO detection. The kinetic temperatures were derived by assuming that the ^{12}CO emission is optically thick and thermalized. This figure indicates that most of the molecular gas in the Gem OB1 complex has kinetic temperatures $\lesssim$10 K after allowing for reasonable levels of subthermal excitation.

with ongoing massive star formation have between 14%–37% of the total mass within relatively high column density lines of sight.

The typical column densities derived for the subregions in the Gem OB1 complex and the subregions without massive star formation are lower by factors of 3–8 compared to the mean column density inferred by Solomon et al. (1987) from virial theorem arguments. Most likely, this difference represents the manner in which clouds were defined by Solomon et al. (1987). Much of the spatial-velocity space of molecular gas in the inner Galaxy is blended at the 1–2 K emission level, so most studies of the inner Galaxy define clouds at a higher threshold level where individual emission peaks are easily segregated (see Lee et al. 1990). As suggested by Figures 2*a* and 2*b*, these regions are preferentially located toward the high column density lines of site and are not representative of the molecular emission in general, In fact, for the 3° × 3° region toward the inner Galaxy studied by Lee et al. (1990), 70% of the emission occurred below the antenna temperature adopted by Solomon et al. (1987) to define clouds. Thus the differences between the average column densities derived in this study and those derived by Solomon et al. (1987) possibly reflect that these authors have preferentially used the higher column densities regions in deriving their average column densities.

Finally, we wish to investigate the kinematics of the molecular gas in the subregions and the Gem OB1 complex. We have separated the motions of the gas into two components derived from (1) the average velocity dispersion of the gas along indi-

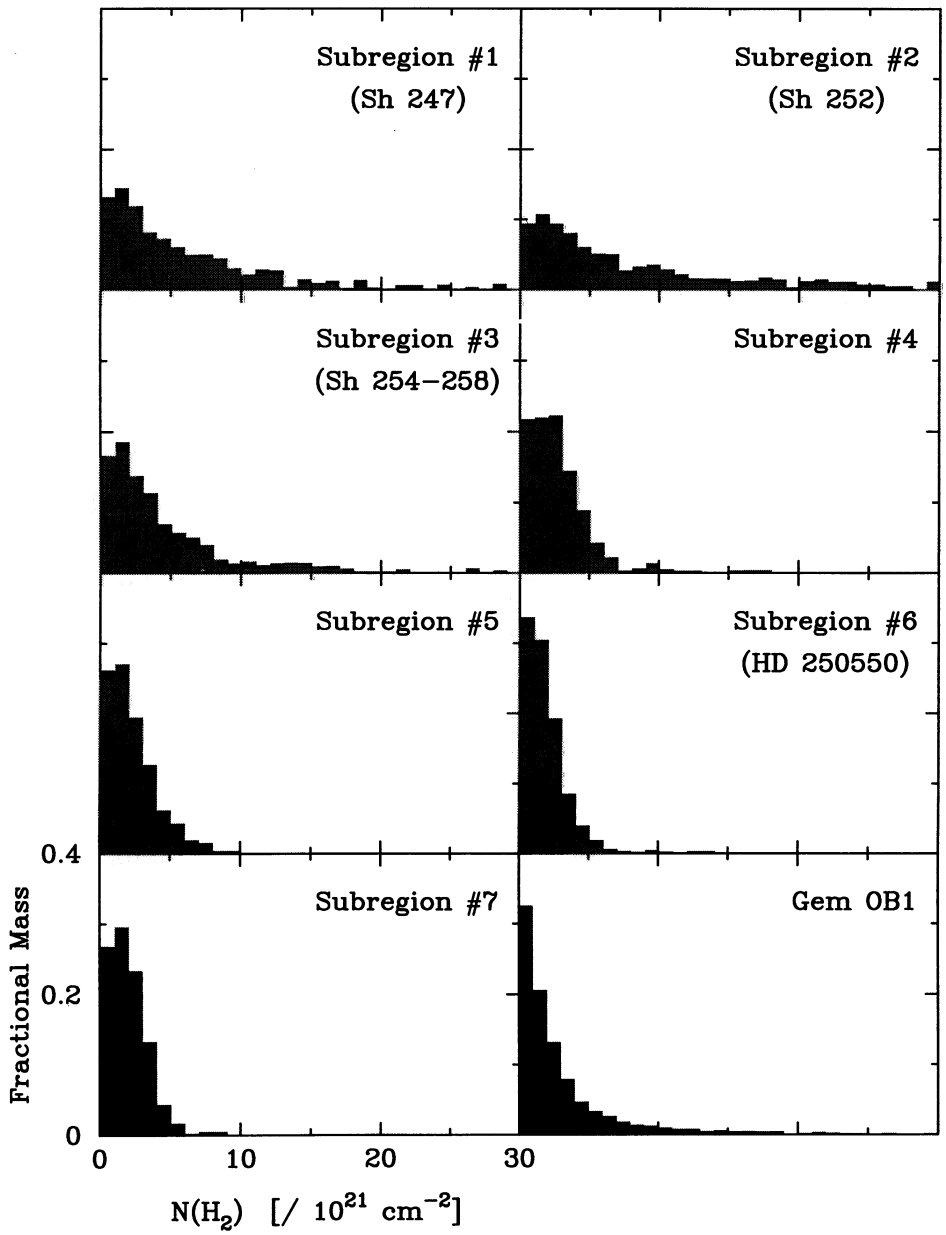

FIG. 12.—Frequency distribution of the H_2 column densities for the seven subregions and for the entire Gem OB1 cloud complex. The column densities were derived from the ^{12}CO and ^{13}CO data using the LTE analysis. The histogram in each panel shows the molecular mass within each column density bin normalized such that the total mass is 1.0. Half of the molecular gas in the Gem OB1 complex is contained in lines of sight with H_2 column densities $\leq 2.0 \times 10^{21}$ cm^{-2}.

vidual lines of sight, and from (2) the dispersion in the velocity centroid from line of sight to line of sight weighted by column density. The average velocity dispersions along individual lines of sight for both ^{12}CO and ^{13}CO are summarized in columns (9) and (10) in Table 2, and the centroid velocity dispersions are listed in column (11) of Table 2. The unusually broad ^{12}CO line widths toward the Sh 247 region are due to the blending of several velocity components in this region (see § 4 and Kömpe et al. 1989). Note that for each of the subregions, the clump to clump motions represented by the centroid velocity dispersion form a significant component of the velocity dispersion of the gas.

Unlike the temperature and column density distributions, it is harder to separate subregions with and without massive star formation by their velocity dispersions. In particular, subregions 4 and 5, which do not have massive star formation, contain on average some of the broadest ^{12}CO and ^{13}CO line widths, which are comparable to those seen in the subregions with massive star formation. The line widths toward the other two subregions without massive star formation (6 and 7) are substantially lower than the other subregions. Interestingly, subregions 4 and 5 appear physically related and may be part of a large arc of molecular gas as described in § 4. The center of curvature of the arc suggests a relationship with the Sh 252 H II region or possibly the heart of the Gem OB1 association (see Fig. 1). While the O6.5 V star in Sh 252 is probably too obscured to have caused such a structure, the collective winds of the OB association could possibly have created such an

arc-shaped feature. In such a scenario, the large line widths maybe due to the turbulent motions as the winds sweep up the molecular gas. This conjecture is somewhat speculative, however, especially since this arc does not contain a large velocity shear which one would expect to accompany a swept up shell of molecular gas.

7.3. *Gravitational Stability*

The analysis in § 6 showed that the energy injected into the molecular gas from the OB stars can account for many of the observed arc shaped structures in the Gem OB1 cloud complex. To determine if this energy is sufficient to disrupt the molecular gas and to make the Gem OB1 complex gravitationally unbound, the kinetic and potential energies of the molecular gas have been calculated for both the designated subregions and the Gem OB1 cloud complex as a whole. Considering for the moment only gravitational forces, the condition for virial equilibrium is that

$$\gamma \equiv \frac{2T}{-W} = 1.0 ,$$

where γ will be referred to as the virial parameter, T is the kinetic energy, and W the gravitational potential energy. Since magnetic fields and external pressures are ignored, γ is more accurately a measure of the importance of self-gravity in the dynamical evolution of the cloud complex. If $\gamma > 1$, the system is gravitationally unbound, and if $\gamma < 1$, it is gravitationally bound.

To estimate the kinetic and potential energies, each line of sight in the molecular line maps were treated as a point mass. The kinetic energy can then be calculated as a discrete sum over the individual pixels as

$$T = \tfrac{3}{2} \sum_{i}^{n} m_i \sigma_i^2 ,$$

where m_i the mass along a line of sight and σ_i is the quadrature sum of the velocity dispersion along the line of sight and the centroid velocity dispersion. The ^{13}CO widths were used in these calculations unless only ^{12}CO was detected along the line of sight. Likewise, the gravitation potential energy can be calculated as

$$W = -G \sum_{i}^{n} \sum_{(j>i)}^{n} \frac{m_i m_j}{|r_i - r_j|} ,$$

where G is the gravitational constant, and $|r_i - r_j|$ the projected distance between any two points in the map. Since the line of sight depth between the various regions is unknown, the absolute value of the gravitational potential is overestimated, and hence, the virial parameter is systematically underestimated within the confines of the other assumptions. This procedure was tested on a model cloud with a spherical, uniform density distribution with a line width such that the cloud obeyed the virial theorem; i.e., $\gamma = 1$. The value of γ obtained from the two-dimensional distribution of column density is 0.67. The results of the virial analysis for the subregions and the Gem OB1 cloud complex are summarized in column (12) in Table 2. The relative values of γ should be considerably more accurate than the absolute values. For example, the absolute value of γ is inversely proportional to the assumed ^{13}CO to H_2 abundance, which observations have shown to be variable between 1×10^{-6} and 2×10^{-6} (Bachiller & Cernicharo 1986).

While the values of γ reported in Table 2 are strictly lower limits, the model of a spherical cloud suggests that the actual values of γ may be no more than 50% larger. Given the uncertainties in both the potential kinetic energy calculations, the fact that γ is within a factor of ~ 2 of unity for each of the subregions and the Gem OB1 complex as a whole suggests that self-gravity remains important in the evolution in each of these regions, and that the rate of star formation has not been sufficient to disperse the complex as a whole.

7.4. *Synthesis*

The above analysis showed that most of the mass of molecular gas in the Gem OB1 complex is relatively cold with kinetic temperatures $\lesssim 10$ K and with column densities of $\lesssim 2 \times 10^{21}$ cm^{-2}. However, there is a stark contrast to the properties of the molecular gas in the subregions with massive star formation and those without. It is only in the subregions with massive star formation where substantial amounts of molecular gas are found that have column densities in excess of 10^{22} cm^{-2} and kinetic temperatures in excess of 10 K, and more specifically, this molecular gas appears to be organized into arcs and ringlike structures.

While intuitively one expects high column density molecular and star formation to strongly correlated, the morphology, physical properties, and in some instances kinematics suggest that many of these high column density regions formed as a result of the interactions of previous massive star-formation events with the ambient molecular gas, and are not remnants of a larger, high column density core that formed the stars in optically visible H II regions. This was most clearly demonstrated for Sh 252, where the size of the H II region, the amount of molecular material contained in the bright rim adjacent to the optical nebula, and the timescales implied by the age of the ionizing star are consistent with models of expanding H II regions. While not all of the arc-shaped and high column density structures are obviously associated with optical nebula, we speculate that most of the high column density regions have formed in an analogous manner. Mid B type stars will not appear with optically visible H II regions, for example, but should have stellar winds with sufficient energy to drive an expanding shell of molecular gas. Thus the high column density regions in the Gem OB1 complex do not appear to have formed by the spontaneous gravitational collapse of the cloud, but instead, by the external compression of the molecular gas by the winds and H II regions from newly formed massive stars.

The salient conclusion from this analysis is that much of the observed structure of the Gem OB1 complex appears to represent the imprint of past star-formation events in the molecular gas. In this model, the expanding bubbles of gas that will naturally arise from H II regions and stellar winds will create high column density molecular gas, which will be the preferred sites of future star-formation events (Carpenter et al. 1995). While this exact same scenario has been proposed for some time now (e.g., Elmegreen & Lada 1977), this study suggests that it may represent one of the primary evolutionary forces in cloud complexes.

8. SUMMARY

We have conducted an extensive investigation of the global cloud structure and star-formation activity in the Gem OB1 molecular cloud complex using a large-scale ^{12}CO($J = 1$–0)

and $^{13}CO(J = 1–0)$ survey covering over 32 deg^2 at 50″ (0.48 pc) sampling. These observations were designed to determine the large-scale morphology and properties of the molecular gas in the Gem OB1 cloud complex, and, as described in a future paper, to determine how the morphology of the gas is related to the current star-formation activity. The primary observational results and conclusions of this work are as follows:

1. The most striking morphological features in the Gem OB1 complex revealed by the ^{12}CO and ^{13}CO images are the series of arclike and ringlike structures found on spatial scales from a few parsecs to 35 pc or more in diameter. The circular shapes and the fact that the interior of the arcs and rings are largely devoid of molecular material, while the outskirts of these structures generally contain strong molecular emission, suggests that these structures formed as a result of sweeping up molecular material. Three of the arc-shaped structures outline the periphery of extended optical H II regions, suggesting that the expansion of the H II region and stellar winds are the principle mechanism responsible for sweeping up the molecular gas. It is proposed, therefore, that the other arc and ring-shaped structures in the Gem OB1 complex have formed in an analogous manner, and that the star responsible for these features are no longer or were never prominently optically visible. While the morphological evidence implicating expansion for the origin of these structures is strong, most of these features do *not* contain kinematic evidence of such a event. Only one ring shows clear evidence for an expanding shell, and only one arc shows a large velocity gradient across the length of the filament which would be expected of an expanding structure.

2. The properties of these arc and ringlike structures were compared with theoretical models of expanding H II regions and wind blown bubbles to investigate whether these structures could plausibly have been formed by these phenomena. The most detailed comparison between theory and observations was made for Sh 252, where it was found that the size of the H II region and the amount of material contained in the rim surrounding Sh 252 are consistent with the dynamics of an expanding H II region. Furthermore, the theoretical models suggest only a small expansion velocity ($\lesssim 2$ km s^{-1}) should be present, which is consistent with the lack of observed expansion motions observed in the region. Similar conclusions were found for the arcs of molecular gas around Sh 247 and Sh 255, although the Sh 247 region would require a higher volume density of H_2 material than assumed for the other regions. The kinetic energies of the other arcs and rings without obvious optical counterparts were estimated to be $\sim 10^{47}$ ergs. These energies are typical of those inferred for molecular outflows from mid to early B type stars, and thus the dynamics of these regions are reasonable from an energetic standpoint.

3. Significant differences in the spatial distribution of the ^{12}CO and ^{13}CO emission were observed. The ^{12}CO emission is more spatially extended than the ^{13}CO emission, which is not just due to the fact that ^{12}CO is more readily detectable, but primarily due to substantial variations in the ratio of ^{12}CO to ^{13}CO integrated intensities. Of the lines of sight with ^{12}CO emission, only 27% have detectable ^{13}CO emission. Based on LVG models, lines of sight with only ^{12}CO emission have densities of a few hundred cm^{-3} and column densities of few $\times 10^{20}$ cm^{-2}. This molecular gas contributes nearly 60% of the total ^{12}CO luminosity, but only an estimated 19% of the molecular mass.

4. The molecular mass of the Gem OB1 complex as estimated from the ^{12}CO and ^{13}CO data is $3.2 \times 10^5\ M_\odot$. The average H_2 density in each of the 7 subregions, which are typically 30 pc in extent, is between 65–120 cm^{-3}, and is independent of whether or not a particular subregion is forming massive stars. These average densities are consistent with what has been found in previous studies, and suggests that the volume filling factor of the molecular material in the subregions is $\lesssim 0.5$. For the Gem OB1 complex as a whole, the average H_2 density is 1.2 cm^{-3}. Assuming that the total H I mass in the Gem OB1 complex is equal to that of H_2, the total proton density of 3.6 cm^{-3} is 4 times that of the average H I volume density (Spitzer 1978). If a "threshold" H_2 column density corresponding to 1 magnitude of visual extinction is required to form the ^{12}CO molecule, as it is suggested both by previous observations and theory, then the mass of molecular gas without ^{12}CO emission may be comparable to the mass inferred from the ^{12}CO and ^{13}CO data.

5. The bulk of the molecular gas has kinetic temperatures $\lesssim 10$ K and half of the total mass of the Gem OB1 complex is contained in lines of sight with H_2 column densities $\leq 2.0 \times 10^{21}$ cm^{-2}. The distinguishing characteristic between regions with and without massive star formation, as traced by optical H II regions and luminous *IRAS* point sources (Carpenter et al. 1995), is the fraction of the total mass with column densities in excess of 10^{22} cm^{-2}. The three regions with massive star formation have between 14% and 37% of their total mass in these relatively high column density lines of sight, while regions without massive star formation have $\leq 2\%$. In general, these high column density lines are associated with warmer molecular gas, and are found along the arc- and ring-shaped structures.

Based on the analysis of these data, we suggest a scenario for the Gem OB1 complex in which the complex consists of relatively diffuse molecular material with low kinetic temperatures and column densities. Once massive stars form, expanding H II regions and stellar winds can sweep up the molecular material to form the arc and filamentary structures that are frequently observed. While such a scenario has been proposed before (e.g., Elmegreen & Lada 1977; see also Norman & Silk 1980), these observations suggest that such mechanisms can be one of the dominant forces shaping the structure of cloud complexes.

We would like to thank Mark Heyer for many interesting discussions on the properties of molecular cloud complexes. This work was supported by NSF grant AST 91-15721 to the Five College Radio Astronomy Observatory. This research has made use of the SIMBAD database, operated at CDS, Strasbourg, France.

APPENDIX

DISTANCE ESTIMATES TO THE GEMINI OB1 CLOUD COMPLEX

While the Gem OB1 cloud complex has been rarely studied as a whole, many of the stars, nebula, and interstellar gas within the cloud complex have been analyzed in great detail. The available distance estimates to the compact H II regions within the molecular

gas converge to 2.0 kpc, which is the adopted distance to the Gem OB1 cloud complex. Some evidence exists that the Gem OB1 association is slightly closer at 1.5 kpc, but this is rather uncertain. This Appendix reviews the available distance estimates to these various features within the region mapped in ^{12}CO and ^{13}CO.

A1. THE GEMINI OB1 ASSOCIATION

Several studies have estimated a distance of $\sim$1.5 kpc to the Gem OB1 association from the photometric or spectroscopic distances to the OB stars (Crawford et al. 1955; Hardie et al. 1960; Humphreys 1978). Haug (1970) suggested, however, that the Gem OB1 association consists of two groups of stars, one at a distance of $\sim$1.2 kpc and the other at $\sim$2 kpc. While the stars show a range of distances from 1 to 2 kpc (see Carpenter 1994), the small number of statistics prevent drawing firm conclusions as to whether there are two distinct associations. The fact that these two possible groups show no spatial segregation on the sky (Carpenter 1994) and that the uncertainty in the distance estimate to Gem OB1 is comparable to other associations in the Galaxy (Walborn 1973; Humphreys 1978) suggest that the Gem OB1 association is a single stellar group. The IC 443 supernova remnant is contained within the Gem OB1 association, and is usually assumed to have a distance of 1.5 kpc as well.

A2. Sh 247

Georgelin (1975, as reported by Kömpe et al. 1989) obtained a spectroscopic distance of 3.8 kpc to the B0 III exciting star for the nebula. Moffat, Fitzgerald, & Jackson (1979) made the same classification, but derived a distance of 3.5 kpc. Lahulla (1987), however, classified the star as a B1 V and determined a photometric distance of 2.2 kpc using an average of four stars within the Sh 247 H II region. Hunter & Massey (1990) made a B0 V classification for the ionizing star and derived a distance of 2.6 kpc. The kinematic distance to Sh 247 is 1.8 $\pm$ 1.4 kpc (Georgelin, Georgelin, & Roux 1973). The uncertainty in this measurement reflects that Gem OB1 lies within 10° of the Galactic anticenter, so that kinematic distances to the individual nebula in Gem OB1 can only serve as a consistency check against other distance estimates and not as a reliable independent measure. Additional evidence for a 2 kpc distance to Sh 247 stems from the apparent physical connection between the Sh 247 and Sh 252 regions as observed in the ^{12}CO and ^{13}CO maps (see § 4 and Kömpe et al. 1989), since Sh 252 has a well determined distance of $\sim$2 kpc (see discussion below).

A3. Sh 252

The distance to HD 42088, the exciting star of Sh 252, has been estimated numerous times from photometric observations. Hardie et al. (1960) derived a distance of 2.0 kpc, Pismis (1970) 1.95 kpc, Georgelin (1975, as reported by Felli, Habing, & Israël 1977) 1.91 kpc, and Humphreys (1978) 2.2 kpc. Distances obtained from main sequence fitting to the Sh 252 cluster are 2.2 $\pm$ 0.3 kpc by Haikala (1984) and 2.3 $\pm$ 0.1 kpc by Chavarría-K, de Lara, & Hasse (1987).

Pismis (1970) found a small cluster of stars $\sim$18′ northeast of the center of the main H II region that had been hidden on previous overexposed images of Sh 252. She derived a distance of 3.5 kpc to this smaller cluster and concluded this was a background object. However, using more recent calibrations of the absolute magnitude scale, the distance to this cluster is revised to 2.1 kpc. In addition, Haikala (1984) and Chavarría-K et al. (1987) derived distances of 2.2 $\pm$ 0.3 kpc and 2.0 $\pm$ 0.1 kpc, respectively, for this cluster. Thus the distance to Sh 252 and the smaller cluster are fairly well established at 2.0 kpc.

A4. Sh 254–258

There is little doubt that all five of these H II regions are at roughly the same distance, as they share the same radial velocities and have independent distance estimates that agree remarkably well. (The agreement occurs for observations within one study, but not necessarily from different studies). Georgelin (1975, as reported by Huang 1985) derived a spectroscopic distance of 2.0 kpc for Sh 254 and 2.3 kpc for Sh 257, while Pismis & Hasse (1976) and Moffat et al. (1979) both estimate a distance of 2.5 kpc. Chavarría-K et al. (1987) derive a photometric distance of 1.9 $\pm$ 0.2 kpc, and Hunter & Massey (1990) derived a distance of 1.2 kpc. The main source of discrepancy in these distance estimates is the uncertainty in the classification of the exciting stars, which varies by up to two subclasses from study to study. By a completely independent method, Armandroff & Herbst (1981) estimated a distance to Sh 255 of 1.92 $\pm$ 0.17 kpc based on star counts. The unweighted average of all of the distances estimates gives 2.0 kpc.

A5. BFS 52

BFS 52 (Blitz et al. 1982) is a small H II region ($\sim$1′ in diameter) at ($l \sim 191.9$, $b \sim 0.8$). While no distance estimates are available for this source, its proximity, common radial velocity, and possible morphological connection (§ 4) with the Sh 254–258 group suggests that BFS 52 is associated with these H II regions.

A6. BACKGROUND OBJECTS: Sh 259

Sh 259 is a small (2′ diameter) H II region that lies $\sim$0°.75 southwest of the Sh 254–258 group. The velocity of the molecular cloud found nearby Sh 259 has a much higher positive velocity (with respect to the local standard of rest) than the Gem OB1 association, Sh 247, Sh 252, and Sh 254–258, and is consistent with the H II region being a distant background source, assuming a flat rotation curve. Moffat et al. (1979) support this assertion, as they estimate a distance of 8.3 kpc to Sh 259 based on spectroscopy of the exciting star. Figure 13 shows a map of the peak ^{12}CO antenna temperature toward this region as observed in the 1 MHz filter banks. The emission toward Sh 259 itself at (α, δ) $\sim$ ($6^h8^m.7$, 17°27′.5) extends only for a few arcminutes. Further to the southeast is a patch of molecular gas $\sim$0°.75 in length at a velocity of $\sim$19 km s^{-1}. The kinematic distance of this material, assuming a flat rotation curve of 220 km s^{-1} and a Galactic center distance of 8.5 kpc for the Sun, is 5.9 $\pm$ 1.0 kpc, corresponding to a linear size scale of $\sim$77 $\pm$ 13 pc. The narrow filament running below the center of Figure 13 occurs at velocities of $\sim$24 km s^{-1}, implying a kinematic distance of 8.1 $\pm$ 1.3 kpc and a size scale of 100 $\pm$ 17 pc. Unless these features have highly peculiar motions, clearly

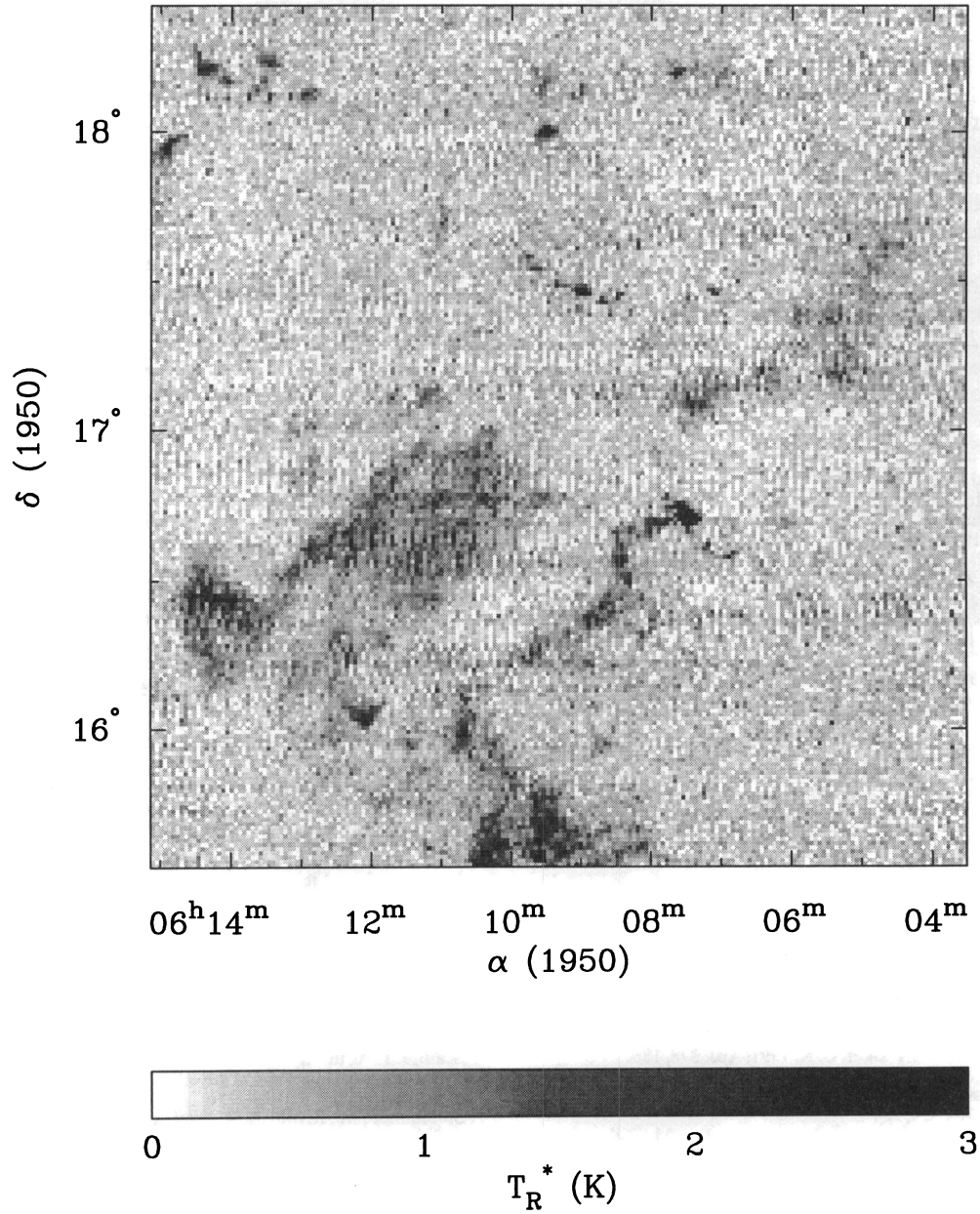

FIG. 13.—Gray-scale image of the ^{12}CO(J = 1–0) emission detected in the 1 MHz filter banks at velocities greater than 16 km s^{-1}. The kinematic distance to these clouds range from 6 to 8 kpc.

extensive quantities of molecular gas are capable of forming at distances up to at least ~16 kpc from the Galactic center. A few emission features appear at velocities of ~13–15 km s^{-1} in the northwest corner of the Gem OB1 cloud complex. Since these features have anomalous velocities compared with the majority of the ^{12}CO emission and are not obviously structurally related to any other features in the maps, they are also considered background molecular clouds.

A7. FOREGROUND OBJECTS: LkHα 208

LkHα 208 is a brilliant bipolar nebulae near the center of the Gem OB1 complex. Finkenzeller & Mundt (1984) quote a distance of 2 kpc to LkHα 208, which would place it within the Gem OB1 cloud complex. However, the optical obscuration toward LkHα 208 is inconsistent with this distance estimate, as LkHα 208 appears along the edge of an opaque spot on the Palomar Sky Survey prints that is much more readily visible than any other region of obscuration in the Gem OB1 cloud complex. Thus while the distance to LkHα 208 is rather uncertain, it is undoubtedly a foreground object.

A8. WESTERN FRONT OF GEMINI OB1

While the distances to the H II regions and the associated molecular material are fairly well established at ~2.0 kpc, no direct distance estimates are available for the molecular material at the western and southern edges of the Gem OB1 complex. The

kinematics cannot resolve the issue since the cloud complex lies close to the anticenter of the galaxy, so most objects will have a velocity with respect to the local standard of rest of ~ 0. It is unlikely that this material gas is local material (i.e., within a few hundred parsecs) since the extinction is not that prevalent on the Palomar Sky Survey prints. Exceptions to this statement are the LkHα 208 region mentioned above, a ring of extinction near $(\alpha, \delta) \sim (6^h12^m, 16°.5)$, and patchy obscuration near around $(\alpha, \delta) \sim (6^h, 17°)$. We have searched for stars with spectroscopic and photometric observations toward the western and southern edges of the Gem OB1 cloud complex in order to determine the distance at which the stars become reddened. The stars that were found do not constrain the distance to any meaningful limits. Since the morphology of the western edge suggests a physical relationship with the Gem OB1 association (see § 4), we will assume that this feature belongs to the Gem OB1 cloud complex.

An indirect distance estimate to the southern edge of the Gem OB1 cloud complex comes from the possible association of the material with the H II region Sh 261. Using the spectroscopic and photometric measurements from Hiltner (1956), the absolute magnitude scale from Humphreys & McElroy (1984), the intrinsic colors from FitzGerald (1970), and the reddening laws from Rieke & Lebofsky (1985), we derived a distance of 1.8 kpc to the exciting star of Sh 261, in close agreement with the distance to Sh 247, Sh 252, and Sh 254–258. Chavarrí-K et al. (1987), however, estimated a distance of 1.0 ± 0.2 kpc using optical photometry and a reddening free index. While we shall take the spectroscopic distance as the best indirect evidence for the distance to this region of the Gem OB1 cloud complex, the distinct possibility remains that this material is foreground gas.

REFERENCES

Abbott, D. C. 1982, ApJ, 263, 723
Armandroff, T. E., & Herbst, W. 1981, AJ, 86, 1923
Bachiller, R., & Cernicharo, J. 1986, A&A, 166, 283
Bally, J., & Lada, C. J. 1983, ApJ, 265, 824
Bally, J., Langer, W. D., Stark, A. A., & Wilson, R. W. 1987, ApJ, 312, L45
Bally, J., & Scoville, N. Z. 1980, ApJ, 239, 121
Barbaro, G., Dallaporta, N., & Fabris, G. 1969, Ap&SS, 3, 123
Blitz, 1978, Ph.D. thesis, Columbia Univ.
———. 1991, in The Physics of Star Formation, ed. C. J. Lada & N. Kylafis (Dordrecht: Kluwer), 1
Blitz, L., Fich, M., & Stark, A. A. 1982, ApJS, 49, 183
Bloemen, H. 1989, ARA&A, 27, 469
Carpenter, J. M. 1994, Ph.D. thesis, Univ. Massachusetts
Carpenter, J. M., Snell, R. L., & Schloerb, F. P. 1995, in preparation
Castor, J., McCray, R., & Weaver, R. 1975, ApJL, 200, L107
Cernicharo, J., & Guélin, M. 1987, A&A, 176, 299
Chiar, J. E., Kutner, M. L., Verter, F., & Leous, J. 1994, ApJ, 431, 658
Chavarría-K, C., de Lara, E., & Hasse, I. 1987, A&A, 171, 216
Crawford, D. L., Limber, N., Mendoza, E., Schulte, D., Steinman, H., & Swihart, T. 1955, ApJ, 121, 24
Dame, T. M., et al. 1987, ApJ, 322, 706
Dickman, R. L. 1978, ApJS, 37, 407
Dickman, R. L., Snell, R. L., & Schloerb, F. P. 1986, ApJ, 309, 326
Dickman, R. L., Snell, R. L., Ziurys, L. M., & Huang, Y.-L. 1992, ApJ, 400, 203
Elmegreen, B. G., & Lada, C. H. 1977, ApJ, 214, 725
Erickson, N. R., Goldsmith, P. F., Novak, G., Grosslein, R. M., Viscuso, P. J., Erickson, R. B., & Predmore, C. R. 1992, IEEE Trans. Microwave Theory and Techniques, 40, 1
Evans, N. J. II, Blair, G. N., & Beckwith, S. 1977, ApJ, 217, 448
Falgarone, E., Phillips, T. G., & Walker, C. K. 1991, ApJ, 378, 186
Felli, M., Habing, H. J., & Israël, F. P. 1977, A&A, 59, 43
Finkenzeller, U., & Mundt, R. 1984, A&AS, 55, 109
FitzGerald, M. P. 1970, A&A, 4, 234
Georgelin, Y. 1975, Ph.D. thesis, Univ. de Provence, Obs. de Marseille
Georgelin, Y. M., Georgelin, Y. P., & Roux, S. 1973, A&A, 25, 337
Goldreich, P., & Kwan, J. 1974, ApJ, 189, 441
Grasdalen, G. L., & Carrasco, L. 1975, A&A, 43, 259
Haikala, L. K. 1984, Ph.D. thesis, Univ. Heidelberg
Hardie, R. H., Seyfert, C. K., & Gulledge, I. S. 1960, ApJ, 132, 361
Haug, U. 1970, A&AS, 1, 35
Heyer, M. H., Morgan, J., Schloerb, F. P., Snell, R. L., & Goldsmith, P. F. 1992, ApJ, 395, L99
Heyer, M. H., Snell, R. L., Morgan, J., & Schloerb, F. P. 1989, ApJ, 346, 220
Hiltner, W. A. 1956, ApJS, 2, 389
Huang, Y.-L. 1985, Ph.D. thesis, Columbia Univ.
Huang, Y.-L., & Thaddeus, P. 1986, ApJ, 309, 804
Humphreys, R. M. 1978, ApJS, 38, 309
Humphreys, R. M., & McElroy, D. B. 1984, ApJ, 284, 565
Hunter, D. A., & Massey, P. 1990, AJ, 99, 846
IRAS Point Source Catalog, Version 2. 1988, Joint *IRAS* Science Working Group (Washington: GPO)
Kömpe, C., Joncas, G., Baudry, A., & Wouterloot, J. G. A. 1989, A&A, 221, 295
Kutner, M. L., & Leung, C. M. 1985, ApJ, 291, 188
Kutner, M. L., & Ulich, B. K. 1981, ApJ, 250, 341
Lada, C. J., & Wooden, W. 1979, ApJ, 232, 158
Lahulla, J. F. 1987, AJ, 94, 1062
Langer, W. D., & Penzias, A. A. 1993, ApJ, 408, 539
Lee, Y., Snell, R. L., & Dickman, R. L. 1990, ApJ, 355, 536
———. 1991, ApJ, 379, 639
———. 1994, ApJ, 432, 167
Leisawitz, D., Bash, F. N., & Thaddeus, P. 1989, ApJS, 70, 731
Maddalena, R. J., & Morris, M. 1987, ApJ, 323, 179
Mazurek, T. J. 1980, A&A, 90, 65
Mead, C., & Kutner, M. C. 1988, ApJ, 330, 399
Moffat, A. F. J., Fitzgerald, M. P., & Jackson, P. D. 1979, A&AS, 38, 197
Norman, C. A., & Silk, J. 1980, ApJ, 238, 158
Panagia, N. 1973, AJ, 78, 929
Patel, N., Goldsmith, P. G., Snell, R. L., Hezel, T., & Xie, T. 1995, ApJ, submitted
Pismis, P. 1970, Bol. Obs. Tonanzintla Tacubaya, 5, 219
Pismis, P., & Hasse, I. 1986, Ap&SS, 45, 79
Polk, K. S., Knapp, G. R., Stark, A. A., & Wilson, R. W. 1988, ApJ, 332, 432
Rieke, G. H., & Lebofsky, M. J. 1985, ApJ, 288, 618
Scalo, J. 1990, in Physical Processes in Fragmentation and Star Formation, ed. R. Capuzzo-Dolcetta, C. Chiosi, & A. Di Fazio (Dordrecht: Kluwer), 151
Sharpless, S. 1959, ApJS, 4, 257
Solomon, P. M., Rivolo, A. R., Barrett, J., & Yahil, A. 1987, ApJ, 319, 730
Spitzer, L., Jr. 1978, Physical Processes in the Interstellar Medium (New York: Wiley)
Stacy, J. G., & Thaddeus, P. 1991, in ASP Conf. Ser. 16, Atoms, Ions, and Molecules: New Results in Spectral Line Astrophysics, ed. A. D. Haschick & P. T. P. Ho (San Francisco: ASP), 197
Tenorio-Tagle, G. 1979, A&A, 71, 59
van Dishoeck, E. F., & Black, J. H. 1988, ApJ, 334, 771
Walborn, N. R. 1973, AJ, 78, 1067
Weaver, R., McCray, R., Castor, J., Shapiro, P., & Moore, R. 1977, ApJ, 218, 377
Xie, T., & Goldsmith, P. 1994, ApJ, 430, 252